 CMES, vol.102, no.1, pp.1-54, 2014

A Smooth Discretization Bridging Finite Element and Mesh-free Methods Using Polynomial Reproducing Simplex Splines

G Devaraj[1], **Shashi Narayan**[1] **and Debasish Roy**[1,2]

Abstract: This work sets forth a 'hybrid' discretization scheme utilizing bivariate simplex splines as kernels in a polynomial reproducing scheme constructed over a conventional Finite Element Method (FEM)-like domain discretization based on Delaunay triangulation. Careful construction of the simplex spline knotset ensures the success of the polynomial reproduction procedure at all points in the domain of interest, a significant advancement over its precursor, the DMS-FEM. The shape functions in the proposed method inherit the global continuity (C^{p-1}) and local supports of the simplex splines of degree p. In the proposed scheme, the triangles comprising the domain discretization also serve as background cells for numerical integration which here are near-aligned to the supports of the shape functions (and their intersections), thus considerably ameliorating an oft-cited source of inaccuracy in the numerical integration of mesh-free (MF) schemes. Numerical experiments show the proposed method requires lower order quadrature rules for accurate evaluation of integrals in the Galerkin weak form. Numerical demonstrations of optimal convergence rates for a few test cases are given and the method is also implemented to compute crack-tip fields in a gradient-enhanced elasticity model.

Keywords: globally smooth shape function, hybrid method, polynomial reproduction, bivariate simplex splines, knot construction, moment matrix invertibility.

1 Introduction

A popular computational technique to numerically evaluate solutions of partial differential equations (PDE) in finite dimensional solution spaces within a Galerkin framework is the finite element method [Ciarlet (1978)]. The subdivision/discretization of the domain of interest into sub-domains/elements is the

[1] Computational Mechanics Lab, Department of Civil Engineering, Indian Institute of Science, Bangalore - 560012, India.
[2] Corresponding Author. E-mail: royd@civil.iisc.ernet.in

most characteristic feature of FEM. It lends FEM ability to approximate complex and irregular domains with element or h refinement, where h denotes the characteristic element size. Another key aspect of FEM is the piecewise polynomial nature of the shape functions constructed locally over these elements. The linear span of the shape functions contains polynomials, an essential ingredient for accurate approximation and convergence of the numerical method. An additional feature is the 'small' compact support of the shape functions leading to a simple description of their construction. The latter two features result in practical computational advantages of easy computations of coefficients of the system of linear or linearized equations and low bandwidth of the corresponding (stiffness) matrix. The above three features of element discretization, piecewise polynomial nature and locally compact support of the FEM shape functions ascribe to FEM its simplicity of implementation, power of approximation and efficiency of computation. Also, they enable the FE space/shape functions to meet the requirements of globally admissible shape functions for the Galerkin weak formulation of the PDE [Ciarlet (1978)]. Still some inherent problems persist in FEM. Most conventional forms of FEM utilize globally C^0 continuous piecewise polynomial shape functions. This results in derivatives of the approximated field variable to be discontinuous across element boundaries thus necessitating adoption of mixed methods or constructing shape functions of global C^n, $n \geq 1$ continuity where the derivatives are required. The former increases the order of the stiffness matrix and imposes additional inf-sup (LBB) conditions on the weak formulation of the mixed system of PDEs leading to practical difficulties. The latter is very difficult for $n \geq 2$ and non-trivial for higher dimensions. On the application side, 'poor' skewed elements resulting from large deformations either rapidly destroy the accuracy of the computation or render the computational procedure inoperable. Problems involving high gradients or discontinuities (e.g. crack initiation and propagation, interface problems) or localized deformation (e.g. shear bands) require either highly refined/dense meshes or non-trivial extensions of the conventional FEM to account for non-local interactions of material points. Each of the requirements for these specialized applications increases the computational cost drastically. Otherwise, adaptive FE procedures need be adopted which bring with them their own issues of accuracy, frequent variable mappings on remeshing and probable mesh bias (e.g. alignment sensitivity in crack and deformation localization) [Li and Liu (2002)].

The emergence of MF methods to numerically solve PDEs provides a means to overcoming the hurdles posed by the above problems [Li and Liu (2002); Nguyen, Rabczuk, Bordas, and Duflot (2008); Fries and Matthies (2003); Belytschko, Krongauz, Organ, Fleming, and Krysl (1996); Babuška, Banerjee, and Osborn (2003)]. Starting with smooth particle hydrodynamics (SPH) in 1977 [Gingold and Mon-

aghan (1977); Lucy (1977)], a myriad of MF methods have been developed since then. To name a few of those employing Galerkin weak formulation (in chronological order), diffuse element method (DEM, 1992) [Nayroles, Touzot, and Villon (1992)], element-free Galerkin method (EFG, 1994) [Belytschko, Lu, and Gu (1994)], reproducing kernel particle method (RKPM, 1995) [Liu, Jun, and Zhang (1995)], hp-clouds (1996) [Duarte and Oden (1996)], partition of unity FEM (PUFEM, 1996) [Melenk and Babuška (1996)], finite point method (FPM, 1996) [Onate, Idelsohn, Zienkiewicz, and Taylor (1996)], free mesh method (FMM, 1996) [Yagawa and Yamada (1996)], meshless local Petrov-Galerkin method (MLPG, 1998) [Atluri and Zhu (1998a)], extended FEM (XFEM, 1999) [Belytschko and Black (1999)] and generalized FEM (GFEM, 2000) [Strouboulis, Copps, and Babuška (2000)]. Other variants include the collocation based MF methods. Instead of an element based discretization, implementations of MF methods require the domain to be populated with 'particles' thus simplifying h-adaptivity. Each particle has its associated compactly supported shape function. For accurate L^2 approximations of $O\left(h^{p+1}\right)$, the approximation space or the linear span of the shape functions should contain the space of all polynomials of degree $\leq p$ i.e. π_p. While conventional FEM shape functions automatically satisfy this requirement, MF shape functions generally do not. Thus, a polynomial reproduction scheme is a crucial ingredient in such methods (MF variants with extrinsic [Duarte and Oden (1996); Ventura, Xu, and Belytschko (2002)] and intrinsic [Fleming, Chu, Moran, Belytschko, Lu, and Gu (1997)] enrichments include other functions e.g. trigonometric, exponential in the shape function and reproduction scheme respectively). Employing compactly supported non-negative C^n kernels in a polynomial reproduction procedure of order p gives compactly supported C^n shape functions containing π_p in their linear span [Han and Meng (2001)]. In principle, MF methods have the capacity to generate shape functions of arbitrary continuity C^n, thus avoiding mixed formulations generally. For large deformation problems, the distortion of particles has less effect on solution accuracy unlike FEM thus requiring no remeshing and avoiding volumetric locking for suitably chosen support sizes [Chen, Pan, Wu, and Liu (1996)]. Higher order continuity also enables easy treatment of crack propagation problems where stress distribution is smoothened near the crack front [Ventura, Xu, and Belytschko (2002); Fleming, Chu, Moran, Belytschko, Lu, and Gu (1997)]. Problems involving localized deformation are solved without the mesh alignment sensitivity encountered in FEM [Li, Hao, and Liu (2000)].

Still, MF methods come with their own disadvantages. The shape functions are typically non-interpolating and lead to difficulties in the imposition of essential boundary conditions unlike FEM [Fernández-Méndez and Huerta (2004)]. Also, the requirement of a mesh is not quite done away in a Galerkin framework since

background integration cells are required to numerically evaluate the integrals. A related problem is the misalignment of the background integration cells with the supports of the shape functions thus leading to integration errors and consequent loss of convergence [Dolbow and Belytschko (1999); Babuška, Banerjee, Osborn, and Li (2008)]. This sensitivity to support size is compounded by the conditions on the geometrical positioning of the particles (and supports) [Han and Meng (2001)] in the polynomial reproduction scheme, leading to costly numerical experiments. Consequently, the support may be neither too 'small' leading to failure of the reproduction procedure nor too 'large' leading to excessive smoothness, misalignment issues and decrease in sparsity of the stiffness matrix. Further, the shape functions are of complex nature (usually rational functions [Nguyen, Rabczuk, Bordas, and Duflot (2008)]) depending on the choice of the kernel function and the polynomial reproducing procedure. The requirement of increased quadrature order reduces the efficiency and accuracy of usual quadrature schemes, designed to be exact for polynomials, and generally renders exact integration nearly impossible. Finally, MF methods are often computationally more expensive and difficult to implement than FEM. For more information regarding specific MF methods, guiding principles, their inherent advantages, disadvantages (and vis-à-vis FEM), remedial methods for the problems encountered, pseudo-codes and a wide range of applications, the reader is referred to the excellent survey articles [Li and Liu (2002); Nguyen, Rabczuk, Bordas, and Duflot (2008); Fries and Matthies (2003); Belytschko, Krongauz, Organ, Fleming, and Krysl (1996); Babuška, Banerjee, and Osborn (2003)] and the references therein.

A 'hybrid' or 'smooth' FEM method explores the possibilities of combining the advantages of FE and MF methods whilst minimizing their disadvantages [Nguyen, Rabczuk, Bordas, and Duflot (2008)]. Methods in which MF methods were coupled to FEM are described in [Belytschko, Organ, and Krongauz (1995); Fernández-Méndez and Huerta (2003); Huerta and Fernández-Méndez (2000); Huerta, Fernández-Méndez, and Liu (2004); Rabczuk, Xiao, and Sauer (2006)]. On the other hand, some proposed hybrid methods are the moving particle FEM (MPFEM) [Hao and Liu (2006)], particle FEM (PFEM) [Idelsohn, Oñate, and Pin (2004)] and reproducing kernel element method (RKEM) [Liu, Han, Lu, Li, and Cao (2004)]. The polynomial reproducing tensor product non-uniform rational B-splines (NURBS)-based parametric method [Shaw and Roy (2008)] utilizing an FE mesh is a recent attempt in this direction wherein a local geometric bijection between the physical and rectangular (cuboidal) parametric domains is developed. The shape functions and their derivatives constructed over the parametric domain transfer their polynomial reproduction property to the physical domain via the bijection. The NURBS-based parametric bridging method [Shaw, Banerjee,

Roy (2008)] extends the technique to domains where at first glance such a geometric map does not exist by constructing the map on a suitable finite decomposition of the domain. Still, this geometric map could induce ill-conditioning in the discretized equations. The parametric domain and consequently the geometric map were avoided in the improvement proposed as the DMS-FEM method [Sunilkumar and Roy (2010)]. In the polynomial reproduction scheme, the tensor product NURBS are replaced with DMS-spline (Dahmen-Michelli-Seidel) kernels [Dahmen, Micchelli, and Seidel (1992)] of degree n having C^{n-1} continuity constructed over a Delaunay triangulation of the physical domain. The derivatives of the shape functions are constructed using the principle espoused in the error reproducing kernel method (ERKM) [Shaw and Roy (2007)]. Another advantage gained was the use of the triangles as background quadrature cells for numerically integrating the discretized equations resulting from the weak formulation. The main constructional aspect of shape functions in DMS-FEM was the generation of knotsets required to be in general position (i.e. non-collinearity of any three knots in 2D). The resulting DMS-spline is supported over the convex hull of the knotset. This method was further extended to 3D with trivariate DMS-splines kernels over tetrahedral meshes and kernels resulting from the tensor product of bivariate DMS-splines with 1D NURBS over triangular prism elements [Sunilkumar, Roy, and Reid (2012)]. The efficacy of DMS-FEM was demonstrated in linear solid mechanics [Sunilkumar and Roy (2010); Sunilkumar, Roy, and Reid (2012)], nearly incompressible and geometrically nonlinear elasto-static problems [Sunilkumar, Roy, and Reid (2012)] and ill-posed problems of wrinkled/slack membranes using 3D nonlinear elasticity [Sunilkumar, Lalmoni, Roy, Reid, and Vasu (2012)]. An important aspect of the DMS-FEM was the use of DMS-splines of order $p+1$ for polynomial reproduction of order p. Further, for points located on the inter-element and domain boundaries, the polynomial reproduction failed sometimes when the degree of DMS-splines and order of polynomial reproduction were the same.

In this work, a set of bivariate simplex spline kernel functions of order p (C^{p-1}) is utilized in place of DMS-splines in the polynomial reproducing scheme of order p such that the reproduction procedure does not fail at any point in the domain of interest. Consequently, the resulting approximation space contains $\pi_{p,2}$. The shape functions inherit the continuity class and compact support of the simplex splines. A major overhaul of the knotset construction procedure of DMS-FEM ensures in addition to the general position of knots, the invertibility of the moment matrix at all points in the domain. An immediate consequence is the considerable reduction of the number of particles required in the proposed method vis-à-vis the DMS-FEM for the same polynomial reproduction order. The shape function derivatives are constructed as in DMS-FEM. Small knot lengths achieve near total alignment

of the shape function supports with triangles in the Delaunay triangulation which also double as the background integration grid akin to DMS-FEM. Moreover, the Delaunay triangulation lends its 'good' properties to the shape function patches, some of which contribute to the FEM-like sparsity of the stiffness matrix. Finally, the proposed method in this work is a 'hybrid' method envisaged to be a variant of DMS-FEM. It is mesh-based due to the fact that the Delaunay triangulation is employed for construction of the shape functions. On the other hand, it possesses the distinctly characteristic feature of an MF method i.e. arbitrary continuity of the shape functions.

The paper is organized as follows. Section 2 describes the bivariate simplex spline reproducing method. Subsequent to preliminary background material, the detailed construction procedures for the bivariate simplex spline kernels are given in Section 2.3. It is followed by a thoroughgoing characterization of the polynomial reproducing aspect of the proposed method in Section 2.4 explained in the setting of a usual polynomial reproducing MF method. Section 3 contains numerical experiments to validate the proposed method followed by relevant conclusions in Section 4. Three Appendices at the end contain relevant material on simplex splines, triangulations and polynomial reproduction essential for the discussions in the paper.

2 The Reproducing Kernel Bivariate Simplex Splines

The basic notations used in the work to follow are first provided below.

$\mathrm{R} = (-\infty, \infty)$ is the set of real numbers. $\mathrm{R}^+ = (0, \infty)$ and $\mathrm{R}_0^+ = \mathrm{R}^+ \cup \{0\}$ are the set of positive and non-negative real numbers respectively. Similarly, $\mathrm{Z}^+ = \{1, 2, ...\}$ and $\mathrm{Z}_0^+ = \mathrm{Z}^+ \cup \{0\}$ are the set of positive and non-negative integers respectively. The first N positive integers are denoted by $J_N = \{i : i \in \mathrm{Z}^+, i \leq N\}$ and, $J_N^0 = J_N \cup \{0\}$. If A is a finite set then $|A|$ is the cardinality of A. If S is a finite dimensional vector space then $\dim(S)$ is the dimension of S. R^d with $d \in \mathrm{Z}^+$ represents the d-dimensional Euclidean space. A nonempty, open, bounded, connected, measurable set with Lipschitz continuous boundary is denoted by $\Omega \subset \mathrm{R}^d$. The boundary of Ω is denoted by $\partial\Omega$ and its interior and closure by Ω° and $\bar{\Omega}$ respectively. $vol_d(\Omega)$ is the d-dimensional volume of Ω, *i.e.* the length ($len(\Omega)$), area ($area(\Omega)$), volume *etc.* of $\Omega \subset \mathrm{R}^d$, $d = 1, 2, 3, ...$ respectively. The characteristic function of Ω is χ_Ω. δ_{ab}, $a, b \in \mathrm{Z}_0^+$ is the Kronecker delta symbol *i.e.* $\delta_{ab} = 1$ iff $a = b$ and $\delta_{ab} = 0$ otherwise. The $d-1$-dimensional hyperplane for $d = 1, 2, 3, \ldots$ is a point, a line, a plane and so on. The canonical basis of R^d is $\{\boldsymbol{e}_i\}_{i=1}^d$ with $\boldsymbol{e}_i \cdot \boldsymbol{e}_j = \delta_{ij}$, and $(\cdot)$ is the usual dot/inner product. $\boldsymbol{x} = (x_1, \ldots, x_d)^T$ denotes the spatial co-ordinates of a generic point in R^d. The length of $\boldsymbol{x} \in \mathrm{R}^d$ is given by the Euclidean norm $\|\boldsymbol{x}\|_2 := \left(\sum_{i=1}^{d} |x_i|^2 \right)^{1/2}$. The *diameter* of a set $S \subset \Omega$

is $diam(S) := \sup_{x,\, y \in S} \{\|\boldsymbol{x}-\boldsymbol{y}\|_2\}$. The support of a function $f : \Omega \to \mathrm{R}$ is supp $f := \overline{\{x \in \Omega : f(x) \neq 0\}}$. A *multi-index* is denoted by $\boldsymbol{\alpha} = (\alpha_1, \ldots, \alpha_d)^T \in \left(\mathrm{Z}_0^+\right)^d$ and its length given by $|\boldsymbol{\alpha}| := \sum_{i=1}^{d} \alpha_i$. Further, $\boldsymbol{\alpha}! = \prod_{i=1}^{d} \alpha_i!$ and $\boldsymbol{x}^{\boldsymbol{\alpha}} := \prod_{i=1}^{d} x_i^{\alpha_i}$. If $\boldsymbol{\beta}$ is also a multi-index, ${}^{\boldsymbol{\alpha}}C_{\boldsymbol{\beta}} := \prod_{i=1}^{d} {}^{\alpha_i}C_{\beta_i}$. The $\boldsymbol{\alpha}^{th}$ order partial differential operator on R^d is $D^{\boldsymbol{\alpha}} := \frac{\partial^{|\boldsymbol{\alpha}|}}{\partial \boldsymbol{x}^{\boldsymbol{\alpha}}} := \frac{\partial^{|\boldsymbol{\alpha}|}}{\partial x_1^{\alpha_1} \ldots \partial x_d^{\alpha_d}}$. The vector space of polynomials of degree up to (*i.e.* less than or equal to) $p \in \mathrm{Z}_0^+$ in d variables on Ω is the set of all their linear combinations *i.e.* $\pi_{p,d}(\Omega) = span\left\{\boldsymbol{x}^{\boldsymbol{\alpha}} : \boldsymbol{x} \in \Omega,\ \boldsymbol{\alpha} \in \left(\mathrm{Z}_0^+\right)^d \text{ and } |\boldsymbol{\alpha}| \leq p\right\}$ with

$$N_{p,d} := \dim\left(\pi_{p,d}(\Omega)\right) = {}^{p}C_d = \frac{(p+d)!}{p!d!}.$$

For ease of handling, the set $\left\{z_{\boldsymbol{\alpha}} \in \mathrm{R} : |\boldsymbol{\alpha}| \leq p,\ p \in \mathrm{Z}_0^+\right\}$ is represented by the vector $z \in \mathrm{R}^{N_{p,d}}$ with the *standard degree lexicographic ordering* on $\boldsymbol{\alpha}$, henceforth referred to as the lexical ordering and given by $(0, \ldots, 0) \prec (1, \ldots, 0) \prec (0, \ldots, 1) \prec (2, \ldots, 0) \prec (1, 1, \ldots, 1) \prec \ldots \prec (0, \ldots, p)$. $\left\{\boldsymbol{x}^{\boldsymbol{\alpha}} : |\boldsymbol{\alpha}| \leq p,\ p \in \mathrm{Z}_0^+\right\}$ is the *complete monomial basis* of $\pi_{p,d}$, represented post lexical ordering by $\boldsymbol{H}(\boldsymbol{x}) \in \mathrm{R}^{N_{p,d}}$. If $\boldsymbol{M}$ is a matrix of order n then $\det \boldsymbol{M}$ and $adj \boldsymbol{M}$ are the determinant and adjugate of $\boldsymbol{M}$ respectively. The element in the i^{th} row and j^{th} column of $\boldsymbol{M}$ is $[\boldsymbol{M}]_{ij}$. $C^0(\Omega)$ is the set of continuous functions on Ω. Similarly, $C^k(\Omega)$ is the set of functions whose k^{th} derivatives are elements of $C^0(\Omega)$. Finally, $C_0^\infty(\Omega)$ denotes the set of $C^\infty(\Omega)$ functions with compact supports in Ω.

2.1 Triangulation of the Domain

Let D be a Delaunay triangulation of $\Omega \subset \mathrm{R}^2$. (For definitions, notations and relevant information for this section, refer to Appendix B). Apart from being an optimal triangulation, certain good properties in a Delaunay triangulation [Hjelle and Dæhlen (2006); Rajan (1994); Rippa (1990)] play an important role in the polynomial reproduction scheme and properties of the resulting shape functions. Without ambiguity, Ω and $\partial\Omega$ are identified with $[\![\mathrm{D}]\!]$ and $\partial\mathrm{D}$ respectively. The elements of T_D are the triangles (2-simplices) in D with their vertices and edges constituting V_D and E_D respectively. The sets $V_\mathrm{D}^B, V_\mathrm{D}^I, E_\mathrm{D}^B$ and E_D^I are the set of *boundary vertices, interior vertices, boundary edges* and *interior edges* respectively. The *F-vector* of D is given by $\boldsymbol{f}_\mathrm{D} = (1, |V_\mathrm{D}|, |E_\mathrm{D}|, |T_\mathrm{D}|)^T$. The elements of T_D are modified into *2-simplices of type p* [Ciarlet (1978)], where p denotes the order of polynomial reproduction. With an abuse of notation, a 2-simplex of type p *i.e.* $L_p(\Delta_2)$ shall be henceforth denoted by Δ and let $\Delta^{(0)}$ denote the set of vertices of Δ. The *P-vector* of D is denoted by $\boldsymbol{p}_\mathrm{D} = \left(0, p_\mathrm{D}^0, p_\mathrm{D}^1, p_\mathrm{D}^2\right)$. It is easy to verify the components of

the *P-vector* of Δ *i.e.* $\boldsymbol{p}_\Delta$ which give the number of vertex, edge and interior nodes in Δ *viz.*, $p_\Delta^0 = 3, p_\Delta^1 = 3(p-1)$ and $p_\Delta^2 = (p-1)(p-2)/2$ respectively and observe that $|\boldsymbol{p}_\Delta| = N_{p,2}$. Denote the set of *nodes* in D by $X_\mathrm{D} = X_\mathrm{D}^V \cup X_\mathrm{D}^E \cup X_\mathrm{D}^T$, where $X_\mathrm{D}^V, X_\mathrm{D}^E$ and X_D^T in the disjoint union constituting X_D are the set of *vertex, edge* and *interior nodes* in D respectively (see Fig. B.1). For $p = 1$ and 2, $X_\mathrm{D}^E = X_\mathrm{D}^T = \emptyset$ and $X_\mathrm{D}^T = \emptyset$ respectively. Clearly, $p_\mathrm{D}^0 = \left|X_\mathrm{D}^V\right| = |V_\mathrm{D}|, p_\mathrm{D}^1 = \left|X_\mathrm{D}^E\right| = p_\Delta^1 |E_\mathrm{D}|/3$ and $p_\mathrm{D}^2 = \left|X_\mathrm{D}^T\right| = p_\Delta^2 |T_\mathrm{D}|$. Also, X_D^I and X_D^B are the set of *interior* and *boundary nodes* in D respectively. The total number of nodes in D is given by $N = |\boldsymbol{p}_\mathrm{D}| = |X_\mathrm{D}|$ which is also the total number of simplex spline kernel functions. For ease of explanation, the indexing in $X_\mathrm{D} = \{\boldsymbol{x}_i\}_{i=1}^N$ is such that the first $\left|X_\mathrm{D}^V\right|$, the next $\left|X_\mathrm{D}^E\right|$ and the remaining $\left|X_\mathrm{D}^T\right|$ elements of X_D give $X_\mathrm{D}^V, X_\mathrm{D}^E$ and X_D^T respectively. The same symbol $\boldsymbol{x}_i$ shall be used to denote the i^{th} node and also the coordinates of the i^{th} node as the context dictates. An important object for the construction of the simplex spline kernels and characterization of the polynomial reproduction of the proposed method is the *local neighborhood* $\aleph(\boldsymbol{x})$ of $\boldsymbol{x} \in \bar{\Omega}$ defined as the set of triangles in T_D(or their union) that have a non-empty intersection with $\boldsymbol{x}$. The nodes and edges of $\aleph(\boldsymbol{x})$ are defined as the set of nodes and edges respectively of all the elements in $\aleph(\boldsymbol{x})$.

2.2 The Bivariate p_M-degree Simplex Spline

For definitions, notations and relevant information for this section, refer to Appendix A. Given a *knotset* $K = \{z_i\}_{i=0}^k \subset \Omega$, the recursive expressions for the bivariate p_M-degree simplex spline $M(\cdot|K)$ are (Eq. (A.3) in Appendix A),

$$M(\boldsymbol{x}|K) = \begin{cases} \chi_{[K)} |D(K)|^{-1} & k = 2 \\ \sum_{i=0}^{2} \lambda_i(U|\boldsymbol{x}) M(\boldsymbol{x}|K \setminus \{\boldsymbol{y}_i\}) & k > 2 \quad \boldsymbol{x} \in \mathrm{R}^2 \end{cases} \tag{1}$$

where $\chi_{[K)}$ is the characteristic function of the *half-open convex hull* of K (see Fig. A.4), $D(K)$ is the *determinant of points* in K, $U = \{\boldsymbol{y}_i\}_{i=0}^d \subset K$ is a *split set* for K (see Fig. A.5) and $\boldsymbol{\lambda}(U|\boldsymbol{x})$s are the *barycentric coordinates* of x with respect to U [Franssen, Veltkamp, and Wesselink (2000)] (see Fig. A.2). If the *knots* are in *general position i.e.* no 3 or more knots are collinear, then $M(\cdot|K)$ is a piecewise polynomial of degree $\leq k-2 = p_M$ and has *optimal smoothness i.e.* $M(\cdot|K) \in C^{p_M-1}(\mathrm{R}^2)$ which is the best possible [Micchelli (1980); Dahmen (1980); Dahmen and Micchelli (1982); Dahmen and Micchelli (1983); Hakopian (1982)], *i.e.*$M(\cdot|K) \in C^{p_M-1}(\mathrm{R}^2) \setminus C^{p_M}(\mathrm{R}^2)$. $M(\cdot|K)$ is non-negative on its support $[K]$ *i.e.* the convex hull of K and if the *knots* are in *general position* then $M(\cdot|K)$ is positive on $[K]^\circ$ [Dahmen and Micchelli (1983)]. The *cut region* for $M(\cdot|K)$ denoted by $\Gamma(M(\cdot|K))$ is the set of line segments joining the knots and the *p-region* for $M(\cdot|K)$ is given by $\Pi(M(\cdot|K)) = [K] \setminus \Gamma(M(\cdot|K))$ [Dahmen and Mic-

chelli (1983)] (see Fig. A.3). In the *p-region*, $M(\cdot|K)$ agrees with a polynomial of degree $\leq p_M$ and therefore belongs to $C^{\infty}(\Pi(M(\cdot|K)))$. For characterization of the continuity of $M(\cdot|K)$ on its cut region, other properties and cases when the knots are *degenerate*, refer Property A.1-6 in Appendix A. In this work, the knotset K is assumed to be in general position and consequently great care is required in knot placement to ensure the above 'best' properties in the constructed simplex spline kernels. Thus, to construct a bivariate simplex spline of degree p_M and having optimal smoothness, the knotset comprises of p_M+3 knots in general position. Further, if the split set U is properly chosen (see sample construction of a bivariate quadratic simplex spline in Fig. A.5), the expression for a higher order bivariate simplex spline in Eq. (1) turns out be a convex combination of three lower degree bivariate simplex splines. Finally, the knotset and simplex spline associated with the i^{th} node are indexed as K_i and $M_i(\cdot|K_i)$ respectively and the set of all simplex spline kernels is denoted by $\mathrm{M} = \{M_i(\cdot|K_i) : i \in J_N\}$.

2.3 Constriction of Bivariate Simplex Spline Kernels on D

The particular indexing in X_{D}, the set of nodes, and M, the set of simplex spline kernel functions, enable the division of M into three useful categories. They are the set of simplex splines associated with the vertex (X_{D}^V), edge (X_{D}^E) and interior (X_{D}^T) nodes and denoted by $\mathrm{M}^V, \mathrm{M}^E$ and M^T respectively. Clearly, the disjoint union $\mathrm{M} = \mathrm{M}^V \cup \mathrm{M}^E \cup \mathrm{M}^T$ holds true. Since the first and major aspect of the construction of a simplex spline is the characterization of its knotset, this section deals with knotset generation akin to relevant sections in [Sunilkumar and Roy (2010)]. The construction procedure for the knotset has two central objectives. *First*, the knotset generated for every simplex spline should be in general position for reasons discussed in the Section 2.2. *Second*, at every point $\boldsymbol{x} \in \bar{\Omega}$, the polynomial reproducing procedure should be successful (see Cases 1-5 in Section 2.4.2). For ease of comprehension, the generation of knotsets elaborated below may be visualized as comprising of the following five general steps *viz.*, (1) construct the initial knotset and (2) ascertain the number of additional knots to be placed, (3) form the required sets of vertices, angles and their dividers for placement of the additional knots, (4) choose a suitable knot length and (5) position and rotate the additional knots by 180°, (6) if required, perturb the knots for correcting degenerate cases and form the final knotset.

2.3.1 Generation of K_i, $i \in \{1,\ldots,|X_{\mathrm{D}}^V|\}$ for construction of simplex splines in M^V

Step 1.0 – Perturb the points in V_{D}^B as follows (see Fig. 1). Bisect the angle subtended interior to Ω by the two boundary edges sharing $\boldsymbol{x} \in V_{\mathrm{D}}^B$. Denote the unit

vector of the bisector by $\boldsymbol{l}$ in the direction from $\boldsymbol{x}$ into Ω. Locate the perturbed $\tilde{\boldsymbol{x}} = \boldsymbol{x} - \delta x \boldsymbol{l}$. This stations $\tilde{\boldsymbol{x}}$ outside Ω. The small quantity δx is chosen to be $k_{\delta x}\boldsymbol{\ell}$ (see *Step 1.4*) with $k_{\delta x} \in [0.1, 0.3]$. Denote the set of perturbed boundary vertices by $\tilde{V}_{\mathrm{D}}^{B} := \left\{\tilde{\boldsymbol{x}} : \boldsymbol{x} \in V_{\mathrm{D}}^{B}\right\}$. Observe that $\bar{\Omega} \subset \left[\tilde{V}_{\mathrm{D}}^{B}\right]$ or more precisely $\bar{\Omega}$ is fully contained in $\left[\tilde{V}_{\mathrm{D}}^{B}\right]$. (It is observed that a similar strategy is adopted in [Meyling (1987)] for treating $\partial\Omega$.)

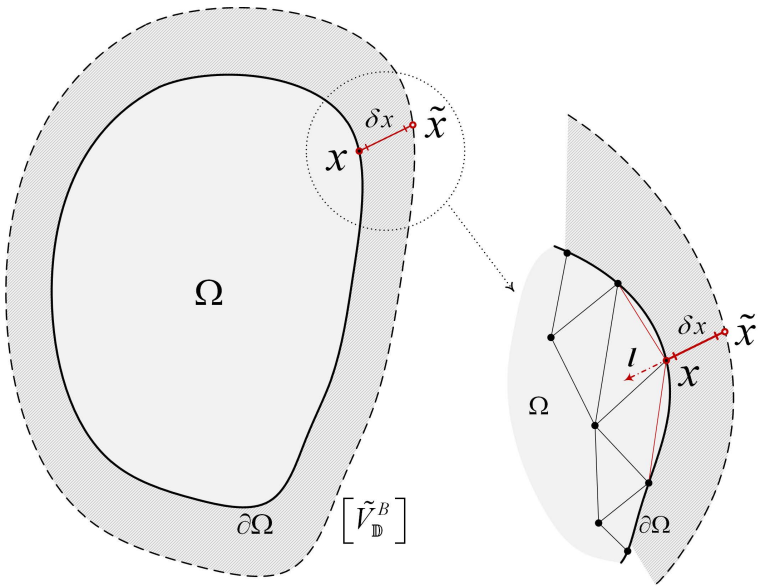

Figure 1: (Step 1.0) Perturbation of $\boldsymbol{x} \in V_{\mathrm{D}}^{B}$ to $\tilde{\boldsymbol{x}}$ outside Ω. Convex hull of the set of perturbed boundary vertices i.e. $\left[\tilde{V}_{\mathrm{D}}^{B}\right]$ shown by the darker region fully contains $\bar{\Omega}$. (The unit vector of the angle bisector $\boldsymbol{l}$ and perturbation length δx are shown exaggerated).

Step 1.1 – Construct $\widehat{K}$ as the set of vertices of the triangles in T_{D} that share $\boldsymbol{x}_i$ (whilst excluding $\boldsymbol{x}_i$), *i.e.* $\widehat{K} = V_{\mathrm{D}} \cap \aleph(\boldsymbol{x}_i) \setminus \{\boldsymbol{x}_i\}$. Points in $\widehat{K}$ that belong to V_{D}^{B} are replaced by their perturbed counterparts in $\tilde{V}_{\mathrm{D}}^{B}$. Let $\boldsymbol{v} = \tilde{\boldsymbol{x}}_i$ if $\boldsymbol{x}_i \in V_{\mathrm{D}}^{B}$ else let $\boldsymbol{v} = \boldsymbol{x}_i$. Denote $\widehat{K}$ by $\left\{\boldsymbol{y}_j\right\}_{j=1}^{\left|\widehat{K}\right|}$ and form the unit vectors $\boldsymbol{l}^j = \left(\boldsymbol{y}_j - \boldsymbol{v}\right) / \left\|\boldsymbol{y}_j - \boldsymbol{v}\right\|_2$. Form the initial set of perturbed points, $\tilde{K} = \left\{\boldsymbol{y}_j + \delta y^{ij}\boldsymbol{l}^j\right\}_{j=1}^{\left|\widehat{K}\right|}$ where $\delta y^{ij} = k_{\delta y}\left\|\boldsymbol{y}_j - \boldsymbol{v}\right\|_2$ with $k_{\delta y} \in [0.01, 0.03]$. Clearly, if $\boldsymbol{x}_i \in V_{\mathrm{D}}^{B}$ then $\left|\tilde{K}\right| = |\aleph(\boldsymbol{x}_i)| + 1$ else $\left|\tilde{K}\right| = |\aleph(\boldsymbol{x}_i)|$. The degree of the simplex spline $M_i\left(\cdot|\tilde{K}\right)$ at this stage is $\left|\tilde{K}\right| - 3$. See Fig. 2(a).

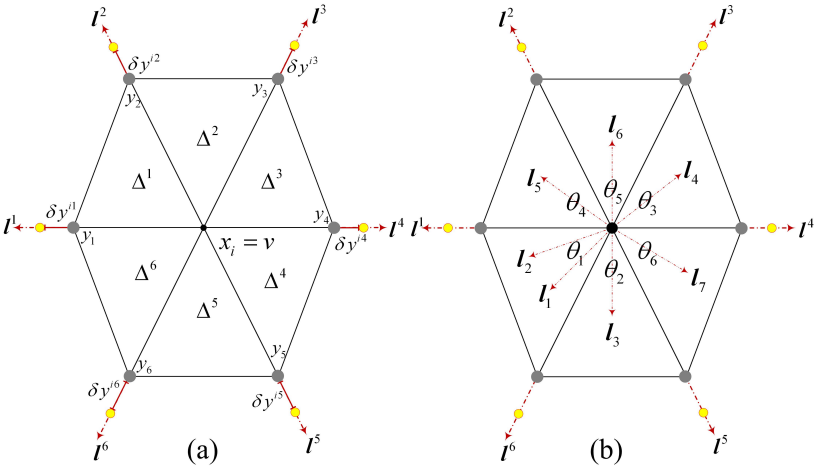

Figure 2: Knotset construction for $\boldsymbol{x}_i \in X_{\mathrm{D}}^V \cap X_{\mathrm{D}}^I$. (a) (Step 1.1) $\aleph(\boldsymbol{x}_i)$ consists of Δ^1 to Δ^6. Set of vertices excluding $\boldsymbol{x}_i$ is $\widehat{K} = \{\boldsymbol{y}_j\}_{j=1}^6$ (grey). Initial knotset of set of six perturbed points $\tilde{K}$ (yellow) along unit vectors $\{\boldsymbol{l}^j\}_{j=1}^6$. (b) (Step 1.3) For illustration purposes, $\bar{p} = 7$ (Step 1.2) which gives $\bar{k} = \bar{r} = 1$. (The unit vectors $\{l^j\}_{j=1}^6$, perturbation distances $\{\delta y^{ij}\}_{j=1}^6$ and unit vectors of the angle dividers $\{l_j\}_{j=1}^7$ are shown exaggerated).

Step 1.2 – If $p > \left|\tilde{K}\right| - 3$, then $\tilde{K}$ needs to be appended with a set of additional $\bar{p} := p - \left|\tilde{K}\right| + 3$ knots denoted by $\bar{K}$ else the knot generation procedure is terminated at this stage with $K_i = \tilde{K}$. But a few pathological cases where $\tilde{\boldsymbol{x}}_i$ (*i.e.* $\boldsymbol{x}_i \in V_{\mathrm{D}}^B$) does not lie in $\left[\tilde{K}\right]^\circ$ even though $p = \left|\tilde{K}\right| - 3$ are corrected by taking $\bar{p} = 1$ so that $\tilde{\boldsymbol{x}}_i \in [\bar{K}]^\circ$. (Since $\deg(\boldsymbol{x}_i) = |\aleph(\boldsymbol{x}_i)| \approx 6, \boldsymbol{x}_i \in V_{\mathrm{D}}^I$ in a Delaunay triangulation, $\left|\tilde{K}\right| - 3$ may be sufficient for $p \leq 3$. The case $p > \left|\tilde{K}\right| - 3$ usually arises when $\boldsymbol{x}_i \in V_{\mathrm{D}}^B$.)

Step 1.3 – The set of $|\aleph(\boldsymbol{x}_i)|$ non-overlapping angles formed between the line segments joining points in $\tilde{K}$ and $\boldsymbol{v}$ at $\boldsymbol{v}$ is denoted by $\{\theta_j\}_{j=1}^{|\aleph(x_i)|}$ and ordered with the descending relation *i.e.* $\theta_r \geq \theta_s$ for $1 \leq r \leq s \leq |\aleph(\boldsymbol{x}_i)|$. Let $\bar{k}$ and $\bar{r}$ be the quotient and remainder of $\bar{p}/|\aleph(\boldsymbol{x}_i)|$ (*i.e.* $\bar{p} = \bar{k}\,|\aleph(\boldsymbol{x}_i)| + \bar{r}, \bar{k}, \bar{r} \in \mathrm{Z}_+^0$) respectively. Now divide the angles $\{\theta_j\}_{j=1}^{\bar{r}}$ equally $\bar{k}+1$ times. Denote its set of unit vectors of the angle dividers as $\{\boldsymbol{l}_j\}_{j=1}^{(\bar{k}+1)\bar{r}}$. Further, divide the remaining angles $\{\theta_j\}_{j=\bar{r}+1}^{|\aleph(x_i)|}$ equally $\bar{k}$ times. Denote its set of unit vectors of the angle dividers as $\{\boldsymbol{l}_j\}_{j=(\bar{k}+1)\bar{r}+1}^{\bar{p}}$. Therefore, if $\bar{p} \leq |\aleph(\boldsymbol{x}_i)|$, then the dividers are the bisectors of

$\left\{\theta_j\right\}_{j=1}^{\bar{p}}$, the largest $\bar{p}$ angles. In all the cases, the direction of the unit vector is from $\boldsymbol{v}$ to the edge opposite the angle it divides. This strategy divides the bigger angles before (and if required, more number of times) than the smaller ones and consequently avoids the near-degenerate inter-crowding of knots by pushing them as radially apart as possible. See Fig. 2(b).

Step 1.4 – A crucial quantity in the placement of the knots is the *knot length*, defined for a knot $\boldsymbol{y} \in \bar{K}$ as $\boldsymbol{\ell}(\boldsymbol{y}) := \|\boldsymbol{y}-\boldsymbol{v}\|_2$. $\boldsymbol{\ell}$ should be not be too small to allow near-degenerate clustering of the knots around $\boldsymbol{v}$. To avoid bizarre and/or large support for the resulting $M_i(\cdot|\cdot)$, $\boldsymbol{\ell}$ should also not be too large. For simplicity of construction, $\boldsymbol{\ell}$ is taken as a constant for all the knots in $\bar{K}$. Define $\boldsymbol{\ell}_{global} := k_f \min\left(\{len(e) : e \in E_{\mathrm{D}}\}\right)$ and $\boldsymbol{\ell}_{local} := k_f \min\left(\left\{len(e) : e \in \Delta^{(1)}, \Delta \in \aleph(\boldsymbol{x}_i)\right\}\right)$ where min is the usual minimum function and k_f is the *knot-factor* usually chosen in the range $0.01-0.1$. Thus, $\boldsymbol{\ell}$ is ideally chosen as $\boldsymbol{\ell}_{local}$ or $\boldsymbol{\ell}_{global}$ for adaptive (or non-uniform) and uniform meshes respectively. $\boldsymbol{\ell}$ may also be chosen based on other suitable criteria; but in this work $\boldsymbol{\ell}_{global}$ is used based on numerical experience with uniform meshes. A different knot length $\boldsymbol{\ell}_b$ can be chosen for knots placed around boundary vertices. For the remainder of the work, unless explicitly specified otherwise, $\boldsymbol{\ell}_b = \boldsymbol{\ell}$ and the symbol $\boldsymbol{\ell}$ shall be used for $\boldsymbol{\ell}_b$ also. The additional $\bar{p}$ knots near (or around) $\boldsymbol{v}$ form the *partial knotcloud* of $\boldsymbol{v}$.

Step 1.5 – Position $\bar{p}$ points at knot length $\boldsymbol{\ell}$ from $\boldsymbol{v}$, one along each $\boldsymbol{l}_j, j \in J_{\bar{p}}$. Thus, the $\bar{p}$ points are given by $\left\{\boldsymbol{v}+\boldsymbol{\ell}\boldsymbol{l}_j\right\}_{j=1}^{\bar{p}}$. Rotate them by 180° about $\boldsymbol{v}$ to get the updated locations $\left\{\boldsymbol{v}-\boldsymbol{\ell}\boldsymbol{l}_j\right\}_{j=1}^{\bar{p}}$. Denote $\left\{\boldsymbol{v}-\boldsymbol{\ell}\boldsymbol{l}_j\right\}_{j=1}^{\bar{p}}$ by K^{part}. For $\boldsymbol{x}_i \in V_{\mathrm{D}}^B$, the rotation operation ensures that the $\bar{p}$ points are not situated in $\aleph(\boldsymbol{x}_i)$ and therefore lie outside $\bar{\Omega}$. See Fig. 3(a).

Step 1.6 – If any 3 or more points in $\tilde{K} \cup K^{part}$ are collinear, then any one (or more) of the points in K^{part} is perturbed by rotating it (anticlockwise) by a small angle $\delta\theta$ (see Fig. 3(b)). $\delta\theta$ is taken as $\sim 1\%$ of the subdivision of the angle which was divided by the angle divider corresponding to the point. Assign the updated coordinates of points in K^{part} to be knots (or locations of knots) in $\bar{K}$. Lastly, $K_i = \tilde{K} \cup \bar{K}$ and the degree of the resulting simplex spline $M_i(\cdot|K_i)$ is p (or $p+1$ for the pathological boundary vertex in *Step 1.2*). Were the procedure terminated at *Step 1.2*, the spline would have degree $\left|\tilde{K}\right| - 3 \geq p$.

Even though *Steps 1.0* and 1.5 are required for generating all the three categories of knotsets, they are onetime activities and therefore not described in the remaining two procedures.

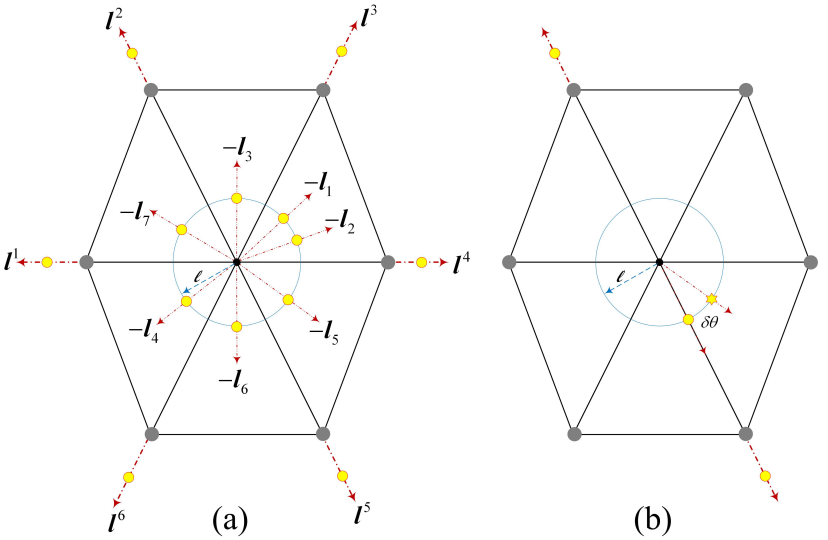

Figure 3: Knotset construction for $\boldsymbol{x}_i \in X_{\mathrm{D}}^V \cap X_{\mathrm{D}}^I$. (a) (Step 1.5) The seven additional knots K^{part} (yellow) along 180° rotated angle dividers $\left\{-\boldsymbol{l}_j\right\}_{j=1}^{7}$ on a circle with radius $\boldsymbol{\ell}$ (Step 1.4) and center $\boldsymbol{v}$. (b) (Step 1.6) Hypothetical case when three knots in $\tilde{K} \cup K^{part}$ are collinear. The knot on the circle is perturbed by $\delta\theta$ to a new position (yellow star). (The unit vectors $\left\{\boldsymbol{l}^j\right\}_{j=1}^{6}$, unit vectors of the angle dividers $\left\{\boldsymbol{l}_j\right\}_{j=1}^{7}$, knot length $\boldsymbol{\ell}$ and perturbation angle $\delta\theta$ are shown exaggerated).

2.3.2 *Generation of K_i, $i \in \left\{\left|X_{\mathrm{D}}^V\right|+1,\ldots,\left|X_{\mathrm{D}}^V\right|+\left|X_{\mathrm{D}}^E\right|\right\}$ for construction of simplex splines in* M^E

Step 2.1 – Construct $\widehat{K}$ as the set of vertices of the triangles in T_{D} that share the edge node $\boldsymbol{x}_i$ *i.e.* $\widehat{K} = V_{\mathrm{D}} \cap \aleph\left(\boldsymbol{x}_i\right)$. Points in $\widehat{K}$ that belong to V_{D}^B are replaced by their perturbed counterparts in $\tilde{V}_{\mathrm{D}}^B$. Denote the vertices of the edge e on which $\boldsymbol{x}_i$ lies as $\boldsymbol{w}_1$ and $\boldsymbol{w}_2$. Let $\boldsymbol{v}_k = \tilde{\boldsymbol{w}}_k \in \tilde{V}_{\mathrm{D}}^B$ if $\boldsymbol{w}_k \in V_{\mathrm{D}}^B$ else let $\boldsymbol{v}_k = \boldsymbol{w}_k$ for $k \in \{1,2\}$. Denote $\widehat{K}\backslash\{\boldsymbol{v}_1,\boldsymbol{v}_2\}$ by $\left\{\boldsymbol{y}_j\right\}_{j=1}^{\left|\widehat{K}\right|-2}$ and form the unit vectors $\boldsymbol{l}^j = \left(\boldsymbol{y}_j - 0.5\left(\boldsymbol{v}_1+\boldsymbol{x}_2\right)\right) / \left\|\boldsymbol{y}_j - 0.5\left(\boldsymbol{v}_1+\boldsymbol{v}_2\right)\right\|_2$ *i.e.* of the bisector of line segment $\overline{\boldsymbol{v}_1\boldsymbol{v}_2}$ passing through $\boldsymbol{y}_j$. Form the set, $\tilde{K} = \{\boldsymbol{v}_1,\boldsymbol{v}_2\} \cup \left\{\boldsymbol{y}_j + \delta y^{ij}\boldsymbol{l}^j\right\}_{j=1}^{\left|\widehat{K}\right|-2}$ with $\delta y^{ij} = k_{\delta y}\left\|\boldsymbol{y}_j - 0.5\left(\boldsymbol{v}_1+\boldsymbol{v}_2\right)\right\|_2$ ($k_{\delta y}$ as in *Step 1.1*) . If $\boldsymbol{x}_i \in X_{\mathrm{D}}^B \cap X_{\mathrm{D}}^E$, *i.e.* $\boldsymbol{x}_i$ lies on a boundary edge, then $\left|\aleph\left(\boldsymbol{x}_i\right)\right| = 1$ and $\left|\tilde{K}\right| = 3$ else $\left|\aleph\left(\boldsymbol{x}_i\right)\right| = 2$ and $\left|\tilde{K}\right| = 4$. Thus, the degree of $M_i\left(\cdot|\tilde{K}\right)$ at this stage is 0 and 1 respectively. See Fig. 4(a).

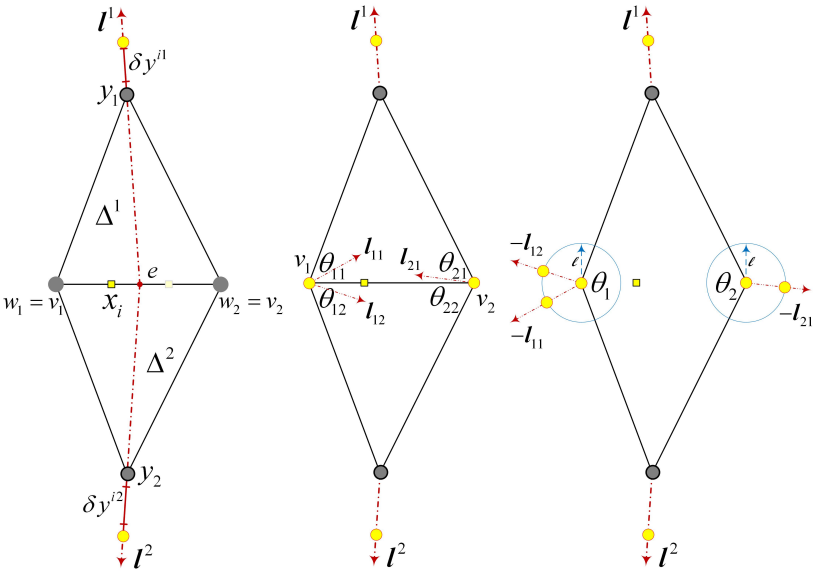

Figure 4: Knotset construction for $\boldsymbol{x}_i \in X_{\mathrm{D}}^E \cap X_{\mathrm{D}}^I$ and $p = 3$. (a) (Step 2.1) $\aleph(\boldsymbol{x}_i)$ consists of Δ^1 and Δ^2. Set of vertices $\widehat{K}$ in $\aleph(\boldsymbol{x}_i)$ is shown in grey. Perturbations of $\{\boldsymbol{y}_j\}_{j=1}^2$ (yellow) are along unit vectors $\{\boldsymbol{l}^j\}_{j=1}^2$. The other edge node on e is shown faded. (b) (Step 2.2) Initial knotset $\tilde{K}$ (yellow) and $m_1/m_2 = 2/1$. (Step 2.3) Construction of angle dividers $\{\boldsymbol{l}_{1j}\}_{j=1}^2$ and $\{\boldsymbol{l}_{21}\}$ of θ_1 and θ_2 respectively. (c) (Step 2.5) The three additional knots in K_1^{part} and K_2^{part} (yellow) along 180° rotated angle dividers $\{-\boldsymbol{l}_{1j}\}_{j=1}^2$ and $\{-\boldsymbol{l}_{21}\}$ on circles with radius $\boldsymbol{\ell}$ (Step 2.4) and centers $\boldsymbol{v}_1$ *and* $\boldsymbol{v}_2$ respectively. (The unit vectors $\{\boldsymbol{l}^j\}_{j=1}^2, \{\boldsymbol{l}_{1j}\}_{j=1}^2, \{\boldsymbol{l}_{21}\}$, perturbation distances $\{\delta y^{ij}\}_{j=1}^2$ and knot length $\boldsymbol{\ell}$ are shown exaggerated).

Step 2.2 – A set of additional p knots $\bar{K}_i$ shall be appended to $\tilde{K}$. The ratio $m_1/m_2 = \|\boldsymbol{x}_i - \boldsymbol{w}_2\|_2 / \|\boldsymbol{x}_i - \boldsymbol{w}_1\|_2$ is the ratio in which $\boldsymbol{x}_i$ divides $len(e)$. Clearly, $m_1 + m_2 = p$. (The ratio m_1/m_2 is also equal to $\lambda_1(e|\boldsymbol{x}_i)/\lambda_2(e|\boldsymbol{x}_i)$ where $\boldsymbol{\lambda}(e|\boldsymbol{x}_i)$ is the barycentric coordinate of $\boldsymbol{x}_i$ with respect to e given by $\boldsymbol{\lambda}(e|\boldsymbol{x}_i) = (\|\boldsymbol{x}_i - \boldsymbol{w}_2\|_2, \|\boldsymbol{w}_1 - \boldsymbol{x}_i\|_2)/len(e)$.)

Step 2.3 – The angles subtended by the line segments joining $\boldsymbol{v}_2$ and $\boldsymbol{v}_1$ with the points in $\tilde{K} \backslash \{\boldsymbol{v}_1, \boldsymbol{v}_2\}$ at $\boldsymbol{v}_1$ and $\boldsymbol{v}_2$ respectively are denoted by $\{\theta_{1j}\}_{j=1}^{|\aleph(x_i)|}$ and $\{\theta_{2j}\}_{j=1}^{|\aleph(x_i)|}$. Define $\theta_k = \sum_{j=1}^{|\aleph(x_i)|} \theta_{kj}, k = \{1,2\}$, the total non-reflex interior an-

gle at $\boldsymbol{v}_k$. Now, divide θ_1 equally m_1 times. Denote its set of unit vectors of the angle dividers as $\left\{\boldsymbol{l}_{1j}\right\}_{j=1}^{m_1}$. Similarly, divide θ_2 equally m_2 times. Denote its set of unit vectors of the angle dividers as $\left\{\boldsymbol{l}_{2j}\right\}_{j=1}^{m_2}$. In both the cases, the direction of the unit vector is into the interior of $\aleph\left(\boldsymbol{x}_i\right)$. See Fig. 4(b).

Step 2.4 – The knot length $\boldsymbol{\ell}$ is chosen for the knots to be placed around $\boldsymbol{v}_1$ and $\boldsymbol{v}_2$ as in *Step 1.4*. Further, $\boldsymbol{v}_1$ and m_1 knots near it form the knotcloud of $\boldsymbol{v}_1$. Similarly, the knotcloud of $\boldsymbol{v}_2$ consists of $\boldsymbol{v}_2$ and m_2 knots near it.

Step 2.5 – Position m_1 points at knot length $\boldsymbol{\ell}$ from $\boldsymbol{v}_1$, one along each $\boldsymbol{l}_{1j}, j \in J_{m_1}$. Post rotation by 180° about $\boldsymbol{v}_1$ gives the updated locations, $\left\{\boldsymbol{v}_1 - \boldsymbol{\ell}\boldsymbol{l}_{1j}\right\}_{j=1}^{m_1}$. Similarly obtain $\left\{\boldsymbol{v}_2 - \boldsymbol{\ell}\boldsymbol{l}_{2j}\right\}_{j=1}^{m_2}$. The rotation operation ensures that the p points are not situated in $\aleph\left(\boldsymbol{x}_i\right)$ and if a vertex of $\aleph\left(\boldsymbol{x}_i\right)$ belongs to V_{D}^B then its partial knotcloud lies outside $\bar{\Omega}$. Denote $\left\{\boldsymbol{v}_1 - \boldsymbol{\ell}\boldsymbol{l}_{1j}\right\}_{j=1}^{m_1}$ and $\left\{\boldsymbol{v}_2 - \boldsymbol{\ell}\boldsymbol{l}_{2j}\right\}_{j=1}^{m_2}$ by K_1^{part} and K_2^{part} respectively. See Fig. 4(c).

Step 2.6 – If any 3 or more points in $\tilde{K} \cup \left(\bigcup_{k=1}^{2} K_k^{part}\right)$ are collinear, then any one (or more) of the points in $\bigcup_{k=1}^{2} K_k^{part}$ is perturbed by rotating it (anticlockwise) by a small angle $\delta\theta$ (see *Step 1.6*). Assign the updated coordinates of points in $\bigcup_{k=1}^{2} K_k^{part}$ to be knots (or locations of knots) in $\bar{K}$. Lastly, $K_i = \tilde{K} \cup \bar{K}$. Thus, the degree of $M_i\left(\cdot|K_i\right)$ is p and $p+1$ depending on $\boldsymbol{x}_i$ being a boundary edge node or an interior edge node respectively.

2.3.3 *Generation of K_i, $i \in \left\{N - \left|X_{\mathrm{D}}^T\right| + 1, \ldots, N\right\}$ for construction of simplex splines in* M^T

Step 3.1 – Construct $\tilde{K}$ as the set of vertices of the triangle in T_{D}in which the interior node $\boldsymbol{x}_i$ lies *i.e.* $\tilde{K} = V_{\mathrm{D}} \cap \aleph\left(\boldsymbol{x}_i\right)$. Points in $\tilde{K}$ that belong to V_{D}^B are replaced by their perturbed counterparts in $\tilde{V}_{\mathrm{D}}^B$. Clearly, $\left|\aleph\left(\boldsymbol{x}_i\right)\right| = 1$ and $\left|\tilde{K}\right| = 3$. Thus, the degree of $M_i\left(\cdot|\tilde{K}\right)$ at this stage is 0. See Fig. 5(a).

Step 3.2 – A set of additional p knots $\bar{K}$ shall be appended to $\tilde{K}$. Denote the vertices of the triangle $\Delta\ (= \aleph\left(\boldsymbol{x}_i\right))$ in which $\boldsymbol{x}_i$ lies as $\boldsymbol{w}_1, \boldsymbol{w}_2$ and $\boldsymbol{w}_3$. The ratio $m_1 : m_2 : m_3 = \lambda_1\left(\Delta|\boldsymbol{x}_i\right) : \lambda_2\left(\Delta|\boldsymbol{x}_i\right) : \lambda_3\left(\Delta|\boldsymbol{x}_i\right)$ is the ratio in which $\boldsymbol{x}_i$ divides $area\left(\Delta\right)$. $\boldsymbol{\lambda}\left(\Delta|\boldsymbol{x}_i\right)$ is the barycentric coordinate of $\boldsymbol{x}_i$ with respect to Δ given by $\boldsymbol{\lambda}\left(\Delta|\boldsymbol{x}_i\right) = \left(area\left(\Delta\boldsymbol{x}_i\boldsymbol{w}_2\boldsymbol{w}_3\right), area\left(\Delta\boldsymbol{w}_1\boldsymbol{x}_i\boldsymbol{w}_3\right), area\left(\Delta\boldsymbol{w}_1\boldsymbol{w}_2\boldsymbol{x}_i\right)\right) / area\left(\Delta\right)$, where (Δabc) denotes a triangle with vertices a, b and c. Clearly, $m_1 + m_2 + m_3 = p$.

Step 3.3 – If $\boldsymbol{w}_k \in V_{\mathrm{D}}^B$ then redefine $\boldsymbol{v}_k = \tilde{\boldsymbol{w}}_k \in \tilde{V}_{\mathrm{D}}^B$ else $\boldsymbol{v}_k = \boldsymbol{w}_k$ for $k \in \{1,2,3\}$ and note that $\tilde{K} = \left\{\boldsymbol{v}_k\right\}_{k=1}^{3}$. The three interior angles of $(\Delta\boldsymbol{v}_1\boldsymbol{v}_2\boldsymbol{v}_3)$ at $\boldsymbol{v}_1, \boldsymbol{v}_2$ and $\boldsymbol{v}_3$ are denoted by θ_1, θ_2 and θ_3 respectively. Now, divide θ_1 equally m_1 times. Denote its set of unit vectors of the angle dividers as $\left\{\boldsymbol{l}_{1j}\right\}_{j=1}^{m_1}$. Similarly divide θ_2 and θ_3 equally m_2 and m_3 times to obtain $\left\{\boldsymbol{l}_{2j}\right\}_{j=1}^{m_2}$ and $\left\{\boldsymbol{l}_{3j}\right\}_{j=1}^{m_3}$ respectively. In all the

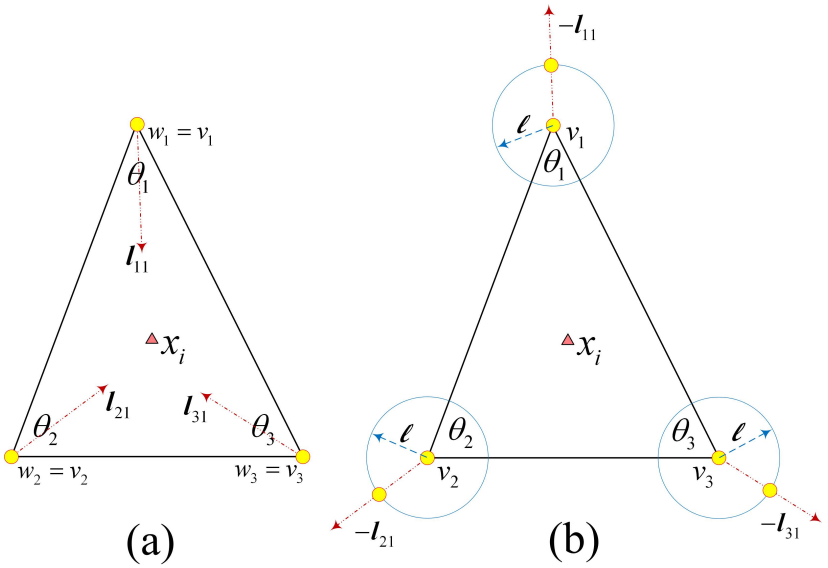

Figure 5: Knotset construction for $\boldsymbol{x}_i \in X_{\mathrm{D}}^T \cap X_{\mathrm{D}}^I$ and $p = 3$. (a) (Step 3.1) Initial knotset $\tilde{K} = \{\boldsymbol{v}_k\}_{k=1}^3$ (yellow). (Step 3.2) $m_1 : m_2 : m_3 = 1 : 1 : 1$ and (Step 3.3) construction of angle dividers $\{\boldsymbol{l}_{11}\}, \{\boldsymbol{l}_{21}\}$ and $\{\boldsymbol{l}_{31}\}$ of θ_1, θ_2 and θ_3 respectively. (b) (Step 3.5) The three additional knots in K_1^{part}, K_2^{part} and K_3^{part} (yellow) along 180° rotated angle dividers $\{-\boldsymbol{l}_{11}\}, \{-\boldsymbol{l}_{21}\}$ and $\{-\boldsymbol{l}_{31}\}$ on circles with radius $\boldsymbol{\ell}$ (Step 3.4) and centers $\boldsymbol{v}_1, \boldsymbol{v}_2$ and $\boldsymbol{v}_3$ respectively. (The unit vectors $\{\boldsymbol{l}_{k1}\}_{k=1}^3$ and knot length $\boldsymbol{\ell}$ are shown exaggerated).

cases, the direction of the unit vector is into the interior of Δ. See Fig. 5(a).

Step 3.4 – The knot length $\boldsymbol{\ell}$ is chosen for the knots to be placed around $\boldsymbol{v}_1, \boldsymbol{v}_2$ and $\boldsymbol{v}_3$ as in *Step 1.4*. Further, the knotcloud of $\boldsymbol{v}_k, k = \{1,2,3\}$ consists of $\boldsymbol{v}_k$ and the m_k knots near it.

Step 3.5 – Position m_1 points at knot length $\boldsymbol{\ell}$ from $\boldsymbol{v}_1$, one along each $\boldsymbol{l}_{1j}, j \in J_{m_1}$. Post rotation by 180° about $\boldsymbol{v}_1$ gives the updated locations, $\left\{\boldsymbol{v}_1 - \boldsymbol{\ell}\boldsymbol{l}_{1j}\right\}_{j=1}^{m_1}$. Similarly obtain $\left\{\boldsymbol{v}_2 - \boldsymbol{\ell}\boldsymbol{l}_{2j}\right\}_{j=1}^{m_2}$ and $\left\{\boldsymbol{v}_3 - \boldsymbol{\ell}\boldsymbol{l}_{3j}\right\}_{j=1}^{m_3}$. The rotation operation ensures that the p points are not situated in Δ and if a vertex of Δ belongs to V_{D}^B then its partial knotcloud lies outside $\bar{\Omega}$. Denote $\left\{\boldsymbol{v}_k - \boldsymbol{\ell}\boldsymbol{l}_{kj}\right\}_{j=1}^{m_k}, k \in \{1,2,3\}$ by K_k^{part} respectively. See Fig. 5(b).

Step 3.6 – If any 3 or more points in $\tilde{K} \cup \left(\bigcup_{k=1}^3 K_k^{part}\right)$ are collinear, then any one (or more) of the points in $\bigcup_{k=1}^3 K_k^{part}$ is perturbed by rotating it (anticlockwise) by a small angle $\delta\theta$ (see *Step 1.6*). Assign the updated coordinates of $\bigcup_{k=1}^3 K_k^{part}$ to be

knots (or locations of knots) in $\bar{K}$. Lastly, $K_i = \tilde{K} \cup \bar{K}$. Thus, the degree of $M_i(\cdot|K_i)$ is p.

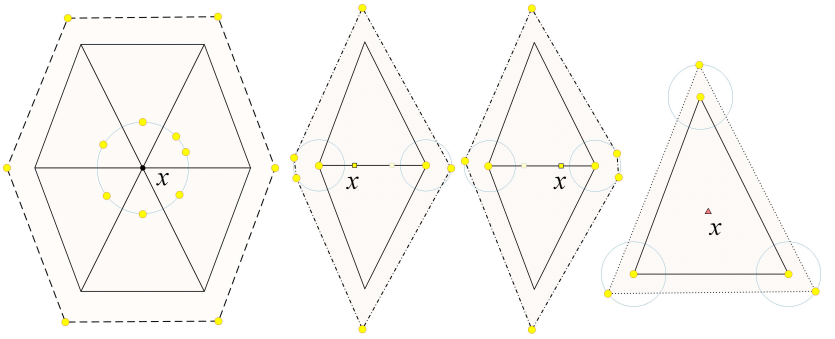

Figure 6: Convex hull of knotset K of node $\boldsymbol{x}$ for (a) M^V, $(b)\mathrm{M}^E$ and (c) M^T simplex spline kernel (shaded area bounded by dotted lines). Observe in each case $\aleph(\boldsymbol{x}) \subset [K]^\circ$. Different knotsets and supports for two edge nodes on the same edge are shown in (b). Knots in and on the circles constitute the knotclouds of their centers.

The remaining task is to construct the individual simplex splines $M_i(\cdot|K_i), i \in J_N$ employing standard and efficient recursive procedures for Eq. (1). The reader is referred to the end of Appendix A where a sample evaluation of a bivariate quadratic simplex spline is depicted. Five general observations on the characteristics of the splines and their supports relevant for the polynomial reproducing framework (see Section 2.4.1) may be made at this stage. It may be noted that there can be many possible scenarios depending on the shape of Ω and the Delaunay triangulation. Here, only the common cases occurring in practice are described. *First*, each knotset is generated to be in general position thus achieving optimal smoothness for the resulting simplex spline. Overall, the elements of M are piecewise polynomials of degree $\leq p$ and have minimum continuity $C^{p-1}\left(\mathrm{R}^2\right)$ (*Steps 1.6, 2.6 and 3.6*) which is inherited by the shape functions post polynomial reproduction. *Second,* for the simplex spline associated with a node $\boldsymbol{x}$, the number of additional knots (*Step 2*) and the strategy employed in the division of angles (*Step 3*) at chosen vertices for their placement ensures that the maximum of the spline occurs near $\boldsymbol{x}$ (or in some sense the spline is centered around $\boldsymbol{x}$). Also, the spline decays monotonically as it recedes from $\boldsymbol{x}$ becoming zero on the boundary of its support rendering them as possible candidates for utilization as kernels in the polynomial reproducing scheme. *Third*, every boundary vertex $\boldsymbol{x} \in V_{\mathrm{D}}^B$ has its partial knotcloud lying outside $\bar{\Omega}$ due to the 180° rotation operation. *Fourth*, the perturbation of the initial knotset $\bar{K}$ (*Steps 1.1*

and 2.1) of a node x helps in ensuring $\aleph(\boldsymbol{x}) \subset [K]^{\circ}$, a crucial property for the polynomial reproducing procedure (see Fig. 6). *Fifth*, similar comment in *Step 1.4* on using other suitable criteria to select ℓ is applicable to the choice of k_f, $k_{\delta x}$, $k_{\delta y}$ and $\delta\theta$ too.

2.4 Polynomial Reproduction with Bivariate Simplex Spline Kernels

2.4.1 Mesh-free method and polynomial reproduction

(For definitions, derivations and relevant information for this section, refer to Appendix C). In the context of the polynomial reproducing mesh-free scheme [Han and Meng (2001), Melenk (2005)], an indexed set of points $X_N := \left\{\boldsymbol{x}_j : \boldsymbol{x}_j \subset \bar{\Omega}\right\}_{j=1}^{N}$ is the set of *particles* and the set of *shape functions* and *patches* associated with X_N are $\Phi_N = \left\{\phi_j\right\}_{j=1}^{N}$ and $\Theta_N := \left\{\Omega_j : \Omega_j = (\text{supp}\varphi_i)^{\circ}\right\}_{j=1}^{N}$ respectively. The set of *patch diameters* is $H_N := \left\{h_j : h_j = diam(\Omega_j)\right\}_{j=1}^{N}$. X_N along with Θ_N constitute a *particle distribution*. The *particle density index* (or *refinement parameter*) h of a particle distribution is a suitable measure of H_N. $u(\boldsymbol{x})$ denotes a *target function* to be approximated and $\tilde{u}(\boldsymbol{x})$ its *particle approximation* *i.e.* $u(\boldsymbol{x}) \sim \tilde{u}(\boldsymbol{x}) = \sum_{j=1}^{N} u(\boldsymbol{x}_j)\,\phi_j(\boldsymbol{x})$. $U_N := \left\{u(\boldsymbol{x}_j)\right\}_{j=1}^{N}$ is the set of *nodal parameters* of the target function. The *approximation space* of the method is defined as $V_N := span(\Phi_N)$. The set of continuous, compactly supported, non-negative functions called the *kernels functions* is $W_N := \left\{w_j\right\}_{j=1}^{N}$. For the reproducing simplex spline method proposed in this paper $X_N := X_{\mathrm{D}}$ *i.e.* the nodes are the particles. A simplex spline $M(\cdot|K)$ in M is an ideal candidate to be utilized as a kernel function because it is non-negative on its compact support $[K]$ (and positive in $[K]^{\circ}$) and belongs to $C^{p-1}\left(\mathrm{R}^2\right)$. Therefore, $W_N := \mathrm{M}$. To proceed further, the *star* of a point $\boldsymbol{x} \in \bar{\Omega}$ is defined as $\mathscr{S}(\boldsymbol{x}) := \left\{j \in J_N : \boldsymbol{x} \in \Omega_j\right\}$ which gives the indices of the shape (or equivalently kernel) functions that have non-zero evaluations at $\boldsymbol{x}$ [Zuppa (2003a)]. Closely related to $\mathscr{S}(\boldsymbol{x})$ is the *star of nodes* at $\boldsymbol{x}$ defined as $\mathrm{S}(\boldsymbol{x}) := \left\{\boldsymbol{x}_j : j \in \mathscr{S}(\boldsymbol{x})\right\}$ in which case x is said to be *covered* by $\left\{\phi_j : j \in \mathscr{S}(\boldsymbol{x})\right\}$. If the requirement that Φ_N reproduces polynomials up to order $p << N$ with respect to X_N is to be satisfied, then the following system of $N_{p,2}$ linear algebraic equations needs to be solved [Han and Meng (2001)],

$$\left[\sum\nolimits_{i\in\mathscr{S}(x)} M_i(\boldsymbol{x}|K_i)\,\boldsymbol{H}(\boldsymbol{x}-\boldsymbol{x}_i)\,\boldsymbol{H}^T(\boldsymbol{x}-\boldsymbol{x}_i)\right]\boldsymbol{c}(\boldsymbol{x}) = \boldsymbol{H}(0), \quad \boldsymbol{x} \in \bar{\Omega}, \tag{2}$$

where the *complete shifted monomial basis* of $\pi_{p,2}$ *i.e.* $\left\{(\boldsymbol{x}-\boldsymbol{x}_i)^{\boldsymbol{\alpha}} : |\boldsymbol{\alpha}| \le p\right\}$ post lexical ordering is $\boldsymbol{H}(\boldsymbol{x}-\boldsymbol{x}_i) \in \mathrm{R}^{N_{p,2}}$ and $\boldsymbol{c}(\boldsymbol{x}) \in \mathrm{R}^{N_{p,2}}$ is the vector of *correction function coefficients*. Define the (*discrete) moment matrix* as $\boldsymbol{M}(\boldsymbol{x}) :=$

$\sum_{i\in\mathscr{S}(x)} M_i(\boldsymbol{x}|K_i)\boldsymbol{H}(\boldsymbol{x}-\boldsymbol{x}_i)\boldsymbol{H}^T(\boldsymbol{x}-\boldsymbol{x}_i)$. Now, if there exists a unique solution $\boldsymbol{c}(\boldsymbol{x}) = \boldsymbol{M}^{-1}(\boldsymbol{x})\boldsymbol{H}(0)$ for Eq. (1) at $\boldsymbol{x}$, then the shape functions at $\boldsymbol{x}$ are given by,

$$\varphi_i(\boldsymbol{x}) = M_i(\boldsymbol{x}|K_i)\boldsymbol{H}^T(\boldsymbol{x}-\boldsymbol{x}_i)\boldsymbol{c}(\boldsymbol{x}), \tag{3}$$

where $\boldsymbol{H}^T(\boldsymbol{x}-\boldsymbol{x}_i)\boldsymbol{c}(\boldsymbol{x})$ is called the *correction function*. The $\boldsymbol{\alpha}^{th}$ derivative ($|\boldsymbol{\alpha}| \leq p-1$) of the shape functions is written as [Shaw and Roy (2007)],

$$\mathscr{D}^{\boldsymbol{\alpha}}\varphi_i(\boldsymbol{x}) = w_i(\boldsymbol{x}-\boldsymbol{x}_i)H(\boldsymbol{x}-\boldsymbol{x}_i)^T\boldsymbol{c}^{\boldsymbol{\alpha}}(\boldsymbol{x}), \tag{4}$$

with $\boldsymbol{c}^{\boldsymbol{\alpha}}(\boldsymbol{x}) = \boldsymbol{M}^{-1}(\boldsymbol{x})\left[D^{\boldsymbol{\alpha}}\boldsymbol{H}(\boldsymbol{x})\right]|_{x=0}$. It is evident from Eq. (2) that the success of the polynomial reproduction scheme at $\boldsymbol{x}$ is equivalent to the success in inverting the moment matrix at $\boldsymbol{x}$. A necessary condition for $\det\boldsymbol{M}(\boldsymbol{x}) \neq 0$ is that $|\mathrm{S}(\boldsymbol{x})| =: \Lambda(\boldsymbol{x}) \geq N_{p,2}$ and a sufficient condition for $\det\boldsymbol{M}(\boldsymbol{x}) \neq 0$ is that $\mathrm{S}(\boldsymbol{x})$ contains a $\pi_{p,2}$-*unisolvent* subset [Han and Meng (2001); Melenk (2005); Zuppa (2003a); Armentano (2001); Zuppa (2003b)]. Various tests are available in literature that seek to determine $\pi_{p,2}$-unisolvency of a set $Z = \{z_i\}_{i=1}^{N_{p,2}} \subset \mathrm{R}^2$ by equivalently determining if Z admits a unique polynomial interpolation in $\pi_{p,2}$ [Ciarlet and Raviart (1972)] *viz.*, verifying the *geometric characterization (GC_p) condition* for Z [Chung and Yao (1977); Jesús and Godés (2006)], verifying Z forms a *Lagrange system of order p*[Gasca and Maeztu (1982); Carnicer and Gasca (2001)] *etc.* If Z satisfies GC_p or forms a Lagrange system of order p then Z admits a unique polynomial interpolation in $\pi_{p,2}$ (or is $\pi_{p,2}$-unisolvent). The GC_p condition for Z is satisfied if for each z_i there exist p distinct straight lines $\{L_{il}\}_{l=1}^{p}$ containing all points in $Z\backslash\{z_i\}$ but not z_i *i.e.* $z_j \in \bigcup_{l=1}^{p} L_{il} \Leftrightarrow i \neq j$. A conjecture proven for $p \leq 5$ that aids in identifying sets that do not satisfy the GC_p condition is as follows; if Z satisfies the GC_p condition then there exists at least one line L such that $|Z \cap L| = p+1$ [Carnicer and Gasca (2001); Hakopian, Jetter, and Zimmermann (2014)]. Even though the GC_p condition is simple in its formulation, in practice it is cumbersome and non-trivial to verify for a given Z and $p \geq 3$. Alternatively, Z forms a Lagrange system of order p if there exists a set of $p+1$ distinct lines $\{L_l\}_{l=0}^{p}$ such that $p+1$ points of Z lie on L_p, p points of Z lie on $L_{p-1}\backslash L_p$, ... and 1 point of Z lies on $L_0\backslash\bigcup_{l=1}^{p} L_l$ [Carnicer and Gasca (2001)]. It may be noted that the first step in the construction of the lines is the conjecture stated above. Still, explicitly known $\pi_{p,2}$-unisolvent configurations of $N_{p,2}$ points are employed to assist in verification of unisolvency of an arbitrary set. All principal lattices of order p of a 2-simplex (*i.e.* $L_p(\Delta_2)$, a 2-simplex of order p) satisfy the GC_p condition (the converse is not true for $p \geq 2$) [Ciarlet (1978); Jesús and Godés (2006)]. These will be the main candidates sought after as subsets of $\mathrm{S}(\boldsymbol{x})$ in *Cases 1-5* that are analyzed next.

2.4.2 Moment matrix invertibility

With a view to characterizing the polynomial reproduction for the proposed method, $\bar{\Omega}$ is partitioned into five sets with their disjoint union giving $\bar{\Omega}$ (see Fig. 7(a)). In other words, a point $\boldsymbol{x} \in \bar{\Omega}$ is in exactly one of the five sets. This enables the complete characterization of the polynomial reproducing property of the shape functions in $\bar{\Omega}$ by validating the necessary and sufficient conditions for invertibility of $\boldsymbol{M}(\boldsymbol{x})$ for a generic point $\boldsymbol{x}$ belonging to each set. Therefore, first partition $\bar{\Omega}$ into two subsets *viz.*, the interior Ω° and boundary $\partial\Omega$ of Ω. Further partition Ω° into three subsets $V_{\mathrm{D}}^{I}, \bigcup_{e\in E_{\mathrm{D}}^{I}} e^{\circ}$ and $\Omega^{\circ}\backslash E_{\mathrm{D}}^{I}$ *viz.*, the interior vertices, the interiors of the interior edges and the interiors of triangles in D. Similarly, partition $\partial\Omega$ into two subsets to obtain V_{D}^{B} and $\partial\Omega\backslash V_{\mathrm{D}}^{B}$ which are the boundary vertices and the interiors of the boundary edges (*i.e.* edges in E_{D}^{B}) respectively. In the description of *Cases 1-5* that follow, the non-zero evaluation at $\boldsymbol{x}$ of the shape (or kernel) function associated with a node is simply referred to as the contribution from the node at $\boldsymbol{x}$. Also, a 2-simplex of order p of a triangle denotes all the nodes (vertex, edge and interior) in that triangle. At this stage, it would be helpful to recall the relevant observations towards the end of Section 2.3 with the remark that only the common scenarios occurring in practice are described. For simplicity, we denote $\Lambda(x)$ by Λ.

Case 1 $(\boldsymbol{x} \in V_{\mathrm{D}}^{I}) --$ Since D is a Delaunay triangulation $\deg(\boldsymbol{x}) = |\aleph(\boldsymbol{x})| \approx 6$. Clearly, $\Lambda = |\aleph(\boldsymbol{x})|\, p(p+1)/2+1 > N_{p,2}$ *i.e.* $\mathrm{S}(\boldsymbol{x})$ contains all the 2-simplices of order p constituting $\aleph(\boldsymbol{x})$. See Fig. 7(b).

Case 2 $(\boldsymbol{x} \in \bigcup_{e\in E_{\mathrm{D}}^{I}} e^{\circ}) --$ Here, $|\aleph(\boldsymbol{x})| = 2$ and $\Lambda \geq |\aleph(\boldsymbol{x})| N_{p,2} - (p+1) > N_{p,2}$ with $\mathrm{S}(\boldsymbol{x})$ containing the two 2-simplices of order p constituting $\aleph(\boldsymbol{x})$. If $\boldsymbol{x}$ lies deep in the interior of the edge then Λ attains the minimum of the range given and if it lies near an edge vertex $\boldsymbol{v}$ then Λ may be greater due to additional contributions from nodes in $\aleph(\boldsymbol{v})$. See Fig. 7(c).

Case 3 $(\boldsymbol{x} \in \Omega^{\circ}\backslash E_{\mathrm{D}}^{I})$ – Here, $\aleph(\boldsymbol{x}) = 1$ and $\Lambda \geq N_{p,2}$ with $\mathrm{S}(\boldsymbol{x})$ containing the 2-simplex of order p that is identified with the triangle in which $\boldsymbol{x}$ lies. If $\boldsymbol{x}$ lies deep in the interior of the triangle then $\Lambda = N_{p,2}$, otherwise Λ may be greater due to additional contributions from nodes in adjacent triangles . See Fig. 8(a).

Case 4 $(\boldsymbol{x} \in V_{\mathrm{D}}^{B}) --$ Depending on the geometry of $\partial\Omega$, $\aleph(\boldsymbol{x})$ can vary from 2 to even 6 or more. Similar to *Case 1,* $\Lambda = |\aleph(\boldsymbol{x})|\, p(p+1)/2+1 > N_{p,2}$ with $\mathrm{S}(\boldsymbol{x})$ containing all the 2-simplices of order p constituting $\aleph(\boldsymbol{x})$. See Fig. 8(b).

Case 5 $(\boldsymbol{x} \in \partial\Omega\backslash V_{\mathrm{D}}^{B}) -$ Clearly, $|\aleph(\boldsymbol{x})| = 1$ and $\Lambda \geq |\aleph(\boldsymbol{x})| N_{p,2} \geq N_{p,2}$ with $\mathrm{S}(x)$ containing the 2-simplex of order p constituting $\aleph(\boldsymbol{x})$. Similar to *Case* 2, if $\boldsymbol{x}$ lies deep in the interior of the edge then Λ attains the minimum of the range given and if it lies near an edge vertex $\boldsymbol{v}$ then Λ may be greater due to additional contributions from nodes in $\aleph(\boldsymbol{v})$. See Fig. 8(c).

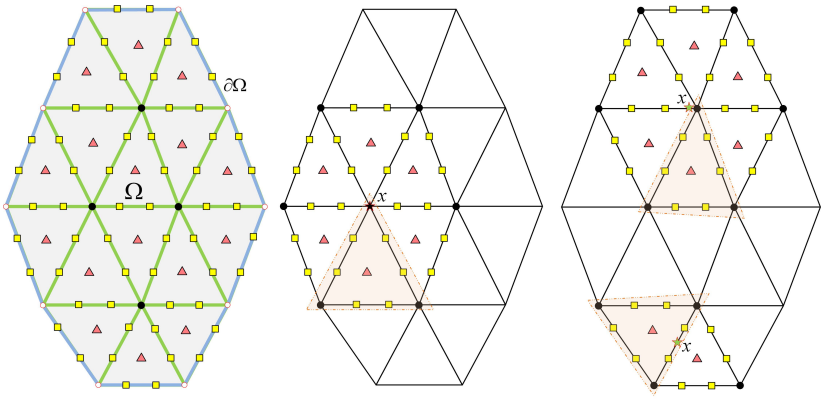

Figure 7: Moment matrix invertibility for simplex splines of degree three and polynomial reproduction of order three at $\boldsymbol{x}$. (a) Five partitions (Cases 1-5) of Ω: 1-black dots, 2-green line segments, 3-grey shaded region, 4-white dots and 5-blue line segments. Nodes in X_{D}^{V} (black dots), X_{D}^{E} (yellow squares) and X_{D}^{T} (rose triangles). (b) Case 1. (c) Case 2. Only the nodes contained in $\mathrm{S}(\boldsymbol{x})$ are shown in (b) and (c). Observe different star(s) of nodes for different locations of $\boldsymbol{x}$ in (c). For each $\mathrm{S}(\boldsymbol{x})$, a $\pi_{3,2}$-unisolvent subset (shaded) is shown.

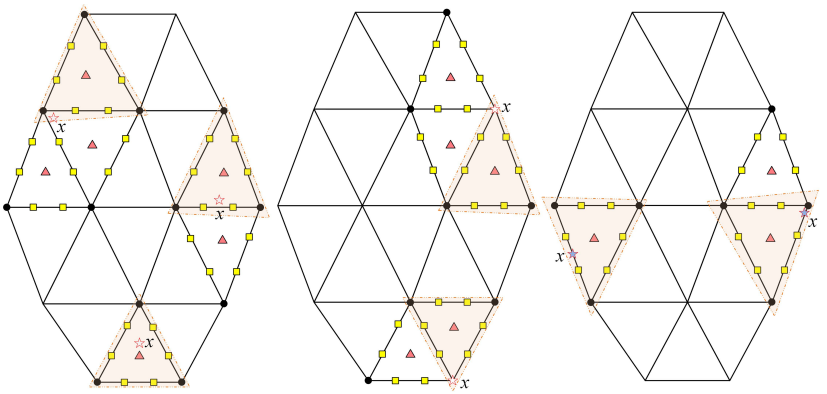

Figure 8: Moment matrix invertibility for simplex splines of degree three and polynomial reproduction of order three at $\boldsymbol{x}$. (a) Case 3 (b) Case 4. (c) Case 5. Only the nodes contained in the star of nodes at $\boldsymbol{x}$ are shown. Observe different $\mathrm{S}(\boldsymbol{x})$ for different locations of $\boldsymbol{x}$. For each $\mathrm{S}(\boldsymbol{x})$, a $\pi_{3,2}$-unisolvent subset (shaded) is shown.

In all the five cases reviewed above, the 2-simplex of order p of any triangle of T_{D} found in $\aleph(\boldsymbol{x})$ can be chosen as the $\pi_{p,2}$-unisolvent subset of $\mathrm{S}(\boldsymbol{x})$. Therefore, $\boldsymbol{M}(\boldsymbol{x})$ is invertible and consequently, the shape functions are computable at all points in $\bar{\Omega}$. For the proposed method, a polynomial reproduction of order $q \in J_{p-1}$is always successful with the same particle distribution since there always exists a principal lattice of order q of a triangle in $\aleph(\boldsymbol{x})$ for all the five cases. Thus, $\mathrm{S}(\boldsymbol{x})$ always contains this lattice as a $\pi_{q,2}$-unisolvent subset. As a corollary, if the simplex spline kernels are of degree $p+1$ then a polynomial reproduction of order p at $\boldsymbol{x} \in \bar{\Omega}$ is always possible. This fact was used in DMS-FEM. If the order of polynomial reproduction is fixed at p then the reduction in the number of degrees of freedom per field variable in the proposed method is $|E_{\mathrm{D}}| + |T_{\mathrm{D}}|(p-1)$ compared to DMS-FEM, which can be considerable while using dense meshes and/or solving system of PDEs. It should be noted that the satisfaction of the geometric conditions for moment matrix invertibility are inherited naturally from the construction of the simplex spline kernels (on the underlying Delaunay triangulation populated with principal lattices of order p) and not by any artificial/trial and error procedure. By the same token, it is easy to analyze and ascertain beforehand, the few problematic locations (if any) for remedial action.

2.4.3 Properties of the approximation space

Next are listed some properties (with possible ramifications) of the approximation space V_N for the proposed method.

(i) *(Polynomial representation/Completeness)* The set of shape functions Φ_N exactly represents (or reproduces) polynomials up to order p in $\bar{\Omega}$ *i.e.* $u(\boldsymbol{x}) = \tilde{u}(\boldsymbol{x}) = \sum_{i=1}^{N} u(\boldsymbol{x}_i)\,\phi_i(\boldsymbol{x})\ \forall u \in \pi_{p,2}\left(\bar{\Omega}\right)$ or equivalently $\pi_{p,2}(\Omega) \subset V_N$ [Han and Meng (2001); Belytschko, Krongauz, Dolbow, and Gerlach (1998)]. For $u(\boldsymbol{x}) \equiv 1$ the polynomial reproduction implies that the shape functions form a partition of unity (PU) *i.e.* $\sum_{i=1}^{N} \phi_i(\boldsymbol{x}) = 1\ \ \forall \boldsymbol{x} \in \bar{\Omega}$.

(ii) *(Continuity)* The shape functions in Φ_N belong to $C^{p-1}\left(\mathrm{R}^2\right)$ [Han and Meng (2001)]. Thus, they form a PU of degree $p-1$ [Babuška and Melenk (1997)].

(iii) *(Compact support)* The set of patches is $\Theta = \left\{[K_i]^{\circ}\right\}_{i=1}^{N}$ since $\mathrm{supp}\varphi_i = \mathrm{supp}M_i(\cdot|K_i) = K_i$ [Han and Meng (2001)].

(iv) *(Non-interpolating nature)* $\phi_i(\boldsymbol{x}_j) \neq \delta_{ij}, i, j \in J_N$. Thus, in general $u(\boldsymbol{x}_i) \neq \tilde{u}(\boldsymbol{x}_i)$. In the framework of numerical solution of PDEs using mesh-free schemes, this deficiency leads to difficulties in imposing essential (or Dirichlet) boundary conditions [Fernández-Méndez and Huerta (2004)]. The present method possesses the knot length as a flexible parameter (*Step 4*). By choosing the knot-factor $k_f \sim$

0.01 and using the fact that Φ_N forms a PU, φ_i, $i \in \left\{1,\ldots,\left|X_{\mathrm{D}}^V\right|\right\}$ becomes 'nearly' interpolating at the vertex nodes $\boldsymbol{x}_i$.

(v) *(Open cover)* Θ_N forms an open cover for $\bar{\Omega}$ due to the perturbation of boundary vertices in *Step 1.0* and 180° rotation operation in *Step 4*. Actually, $\bar{\Omega} \subset \left[\bigcup_{j=1}^{N} \Omega_j\right]^{\circ}$. See Fig. 1.

Let h^i denote the maximum of the diameters of the triangles in $\aleph(\boldsymbol{x}_i)$ (equal to the length of the longest edge in $\aleph(\boldsymbol{x}_i)$). It is easy to verify that $h_i \leq 2\left(h^i + \boldsymbol{\ell} + \max\left\{\delta y^{ij}\right\}\right)$ and $\leq h^i + 2\boldsymbol{\ell}$ for $j \in \left\{1,\ldots,N-\left|X_{\mathrm{D}}^T\right|\right\}$ and $\left\{N-\left|X_{\mathrm{D}}^T\right|+1,\ldots,N\right\}$ respectively. In any case $h_i < 3h^i$ for $i \in J_N$ due to the particular choices of $k_{\delta y}$ and k_f (*Steps 1.1, 1.4* and2.1). Define $h_{\min} := \min H_N$ and $h_{\max} := \max H_N$. Another quantity of interest is $n(i) := \left\{j : \Omega_i \cap \Omega_j \neq \emptyset\right\}$ for $i \in J_N$. The remaining properties are primarily due to the good features of the underlying Delaunay mesh.

(vi) *(Local patch comparability/quasi-uniformity* [Melenk (2005); Han and Meng (2001)]) Θ_N is locally comparable *i.e.* there exists $C \in \mathrm{R}^+$ such that $C^{-1} \leq h_i h_j^{-1} \leq C$, for all $i \in J_N$ and $j \in n(i)$. This is due to the fact that locally a Delaunay triangulation consists of uniform triangles *i.e.* $h^i \approx h^j$ and $h_i \approx h_j$ implying $h_i h_j^{-1}$ is of $O(1)$. Meshes with $h_{\min} \approx h_{\max}$ are quasi-uniform *i.e.* $\bar{C}^{-1} \leq h_i h_j^{-1} \leq \bar{C}$ for all $i, j \in J_N$. In such cases a particle density index h can be found such that $\tilde{C}^{-1} \leq h_i h^{-1} \leq \tilde{C}$ for all $i \in J_N$ [Han and Meng (2001)].

(vii) *(Finite overlap* [Babuška and Melenk (1997); Zuppa (2003a)]) Θ_N satisfies the finite pointwise overlap condition *i.e.* there exists $M^* \in \mathrm{Z}^+$ such that $\Lambda(\boldsymbol{x}) \leq M^*$ for all $\boldsymbol{x} \in \bar{\Omega}$. $M^* = \max\left(\left|\aleph(\boldsymbol{x})\right|\right) p(p+1)/2 + 1$ with $\boldsymbol{x} \in V_{\mathrm{D}}^I$ since maximum overlap occurs at interior vertex nodes. Θ_N also satisfies the finite patch overlap condition *i.e.* there exists $M^{\Theta} \in \mathrm{Z}^+$ such that $|n(i)| \leq M^{\Theta}$ for all $i \in J_N$. The lower bounds for $\Lambda(\boldsymbol{x})$ are important for moment matrix invertibility, as demonstrated in Section 2.4.2. On the other hand, the upper bounds M^* and M^{Θ} directly affect the sparsity of the stiffness matrix. With small knot length and suitable quadrature rule (sampling points not near the boundary of the triangles), the number of non-zero entries in a row of the stiffness matrix does not exceed M^*.

The above properties iii, v, vii and the fact that each patch contains a 2-simplex make $(X_N,\ \Theta_N)$ an *admissible particle distribution* [Liu, Li, and Belytschko (1997)]. Finally, a remark on numerical integration of the weak form for the proposed method in the context of MF methods. It is well known that misalignment of the patches with the background integration grid results in a loss of accuracy and convergence. In the proposed method, the triangles in D serve as the integration cells similar to DMS-FEM. And since with small knot length the patches as well as their intersections nearly coincide with the triangles, misalignment and consequent

issues are ameliorated [Sunilkumar and Roy (2010)]. An implication being the use of a low order quadrature schemes.

3 Numerical Results

For numerical convergence studies, the particle approximation $\tilde{u}(\boldsymbol{x})$ to the target function $u(\boldsymbol{x})$ is subscripted with the characteristic mesh length $h := \max\left\{h^i : i \in J_N\right\}$ and is denoted by $\tilde{u}_h(\boldsymbol{x})$. In all the cases, $k_{\delta x}$ =10%, k_f =1%, $k_{\delta y} = 1\%$ and the degree of simplex spline p and the polynomial reproduction order are same. The domain of interest is $\Omega_a = [0,1]^2$ for the problems in Section 3.1 – 3.3. The details of the discretization/refinement of the triangulation of Ω_a using the EasyMesh package [Niceno (2001)] are summarized in Table 1. The L^2 and H^1 norms of the absolute interpolation (or approximation) error $e_h := u(\boldsymbol{x}) - \tilde{u}_h(\boldsymbol{x})$ are plotted on log-log scales in each case.

Table 1: Domain discretization details of $\Omega_a = [0,1]^2$ for problems in Sections 3.1, 3.2 and 3.3.

Mesh#	h	$\lvert V_{\mathrm{D}}\rvert$	$\lvert E_{\mathrm{D}}\rvert$	$\lvert T_{\mathrm{D}}\rvert$	$N(p=1)$	$N(p=2)$	$N(p=3)$
1	0.5050762697701940	12	25	14	12	37	76
2	0.2841141401254610	31	74	44	31	105	223
3	0.1511668579844160	91	238	148	91	329	715
4	0.0771705470110333	337	944	608	337	1281	2833
5	0.0378521051300686	1256	3637	2382	1256	4893	10912

3.1 Approximation of polynomial, exponential and sinusoidal functions

To show the reproduction properties of the proposed method, polynomials of suitable degree are approximated via the shape functions. To be more precise, $u(\boldsymbol{x}) = (x+y)^p$ is chosen as the target function for approximation when the order of polynomial reproduction is p. Fig. 9 shows the behavior of the error in L^2 and H^1 norms for the meshes in Table 1 and $p = 1$, 2 and 3.

An exponential target function $u(\boldsymbol{x}) = e^{(x+y)}$ is chosen to study the behaviour of the approximant $\tilde{u}_h(\boldsymbol{x})$. Fig. 10 shows the convergence characteristics of the interpolation error and the slope of the individual line segments of the error plot is tabulated in Table 2. It is noted that the convergence rates are nearly equal to the optimal rates of $p+1$ and p for L^2 and H^1 norms of interpolation error respectively.

Next, a sinusoidal target function $u(\boldsymbol{x}) = \sin(\pi(x+y))$ is chosen. Fig. 11 shows the convergence characteristics of the interpolation error and the slope of the indi-

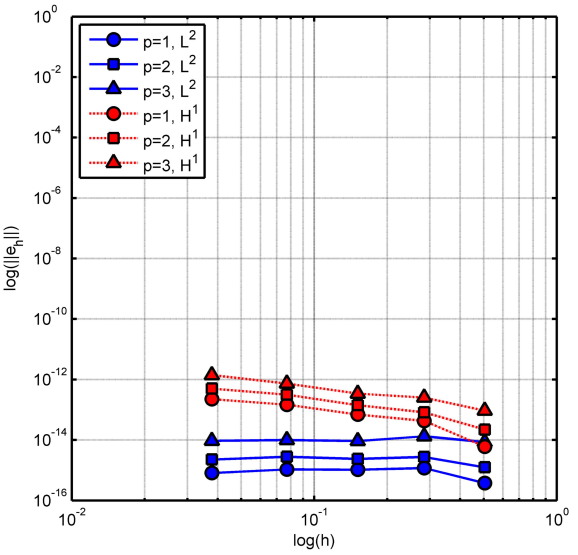

Figure 9: Absolute errors for polynomial reproduction of $u(\boldsymbol{x}) = (x+y)^p$ in L^2 and H^1 norms for Ω_a.

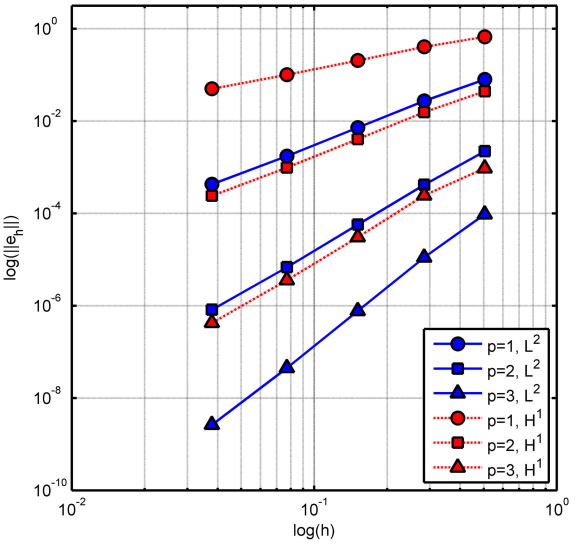

Figure 10: Absolute errors for approximation of $u(\boldsymbol{x}) = e^{(x+y)}$ in L^2 and H^1 norms for Ω_a.

Table 2: Absolute errors for approximation of $u(\boldsymbol{x}) = e^{(x+y)}$ in L^2 and H^1 norms for Ω_a.

Mesh#	$\|e_h\|_{L^2(\Omega_a)}$			$\|e_h\|_{H^1(\Omega_a)}$			Convergence Rate					
							L^2			H^1		
	$p=1$	2	3	1	2	3	1	2	3	1	2	3
1	7.98274E-02	2.22985E-03	9.58986E-05	6.71708E-01	4.43964E-02	9.58529E-04	-	-	-	-	-	-
2	2.73849E-02	4.18457E-04	1.11664E-05	4.06110E-01	1.56352E-02	2.46824E-04	1.86	2.91	3.74	0.87	1.81	2.36
3	7.23736E-03	5.73296E-05	7.75320E-07	2.05560E-01	4.08182E-03	3.06526E-05	2.11	3.15	4.23	1.08	2.13	3.31
4	1.74943E-03	6.82447E-06	4.51432E-08	1.01017E-01	9.86653E-04	3.59242E-06	2.11	3.17	4.23	1.06	2.11	3.19
5	4.28945E-04	8.20914E-07	2.64675E-09	4.99860E-02	2.41085E-04	4.25745E-07	1.97	2.97	3.98	0.99	1.98	2.99

vidual line segments of the error plot is tabulated in Table 3. Near optimal convergence rates are noted here too.

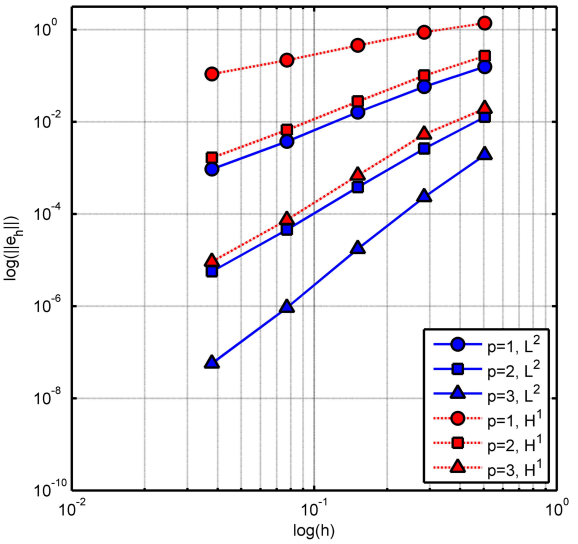

Figure 11: Absolute errors for approximation of $u(\boldsymbol{x}) = \sin(\pi(x+y))$ in L^2 and H^1 norms for Ω_a.

For the two PDE problems that follow, the actual solution is denoted by $u(\boldsymbol{x})$ while the computed solution is denoted by $\widehat{u}_h(\boldsymbol{x})$. Similar to the latter cases, here too the L^2 and H^1 norms of the absolute solution error $e_h = e^{(x+y)} - \widehat{u}_h(\boldsymbol{x})$ are analyzed for studying the convergence. Further, the symmetrical triangle 1 point, 6 point and 6 point quadrature rules [Dunavant (1985)] are used for numerical integration of the Galerkin weak form for p =1, 2 and 3 respectively. Likewise, 1 point, 4 point and 4 point Gauss-Legendre quadrature rules are used for numerical integration of boundary integrals for p =1, 2 and 3 respectively. Thus, as reasoned at the end of Section 2, higher order quadrature schemes need not be utilized in the proposed method.

3.2 A pure Neumann boundary value problem

A Helmholtz like equation is solved for pure Neumann boundary conditions *i.e.*

$$-\Delta u + u = f \quad \text{in} \quad \Omega \quad \text{with} \quad \frac{\partial u}{\partial \boldsymbol{\nu}} = g \quad \text{on} \quad \partial\Omega \tag{5}$$

Table 3: Absolute errors for approximation of $u(\boldsymbol{x}) = \sin(\pi(x+y))$ in L^2 and H^1 norms forΩ_a.

Mesh#	$\|e_h\|_{L^2(\Omega_a)}$			$\|e_h\|_{H^1(\Omega_a)}$			Convergence Rate					
							L^2			H^1		
	$p=1$	2	3	1	2	3	1	2	3	1	2	3
1	1.57398E-01	1.27811E-02	1.92194E-03	1.39287E+00	2.68135E-01	1.92540E-02	-	-	-	-	-	-
2	5.80862E-02	2.62019E-03	2.34399E-04	8.82081E-01	1.00793E-01	5.36667E-03	1.73	2.75	3.66	0.79	1.70	2.22
3	1.62677E-02	3.82854E-04	1.75588E-05	4.56596E-01	2.76437E-02	6.90088E-04	2.02	3.05	4.11	1.04	2.05	3.25
4	3.75046E-03	4.59189E-05	9.30935E-07	2.18335E-01	6.67804E-03	7.47902E-05	2.18	3.15	4.37	1.10	2.11	3.30
5	9.40371E-04	5.67012E-06	5.75398E-08	1.09426E-01	1.66220E-03	9.26383E-06	1.94	2.94	3.91	0.97	1.95	2.93

The actual solution is assumed to be $u(\boldsymbol{x}) = e^{(x+y)}$ and consequently f and g are known functions. Fig. 12 shows the convergence characteristics of the solution error and the slope of the individual line segments of the error plot is tabulated in Table 4. Similar to the approximation characteristics, near optimal convergence rates are observed here.

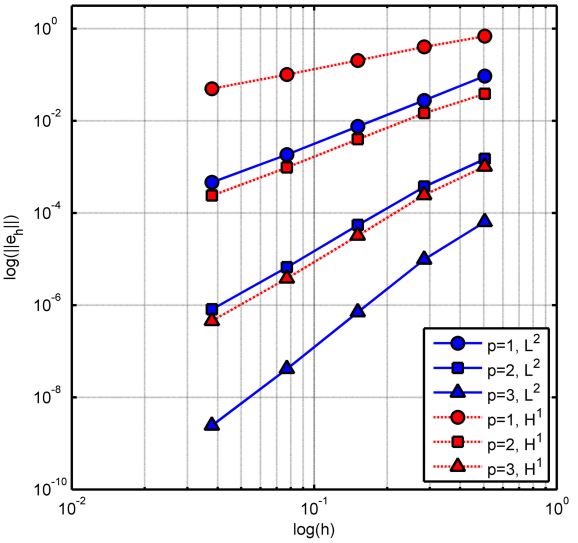

Figure 12: Absolute solution errors for the pure Neumann problem in L^2 and H^1 norms for Ω_a.

3.3 Poisson's equation with Dirichlet boundary condition

To test the proposed method with a PDE with Dirichlet boundary conditions, the Poisson's equation is solved numerically.

$$-\Delta u = f \quad \text{in} \quad \Omega \quad \text{with} \quad u = g \quad \text{on} \quad \partial\Omega \tag{6}$$

Similar to the pure Neumann problem, the actual solution is assumed to be $u(\boldsymbol{x}) = e^{(x+y)}$ and consequently f and g are known functions. The Dirichlet boundary conditions are imposed using the penalty method. To get desired convergence characteristics (*i.e.* optimal rates) the penalty factor is taken to be $10^4 h_m^{-p}$ where $h_m := \min\left\{h^i : i \in J_N\right\}$ based on [Fernández-Méndez and Huerta (2004)]. Fig. 13 shows the convergence characteristics of the solution error and the slope of the individual line segments of the error plot is tabulated in Table 5. Finally, near optimal rates are achieved here too.

Table 4: Absolute solution errors for the pure Neumann problem in L^2 and H^1 norms for Ω_a.

Mesh#	$\|e_h\|_{L^2(\Omega_a)}$			$\|e_h\|_{H^1(\Omega_a)}$			Convergence Rate					
							L^2			H^1		
	$p=1$	2	3	1	2	3	1	2	3	1	2	3
1	9.38091E-02	1.49036E-03	6.42862E-05	6.90081E-01	3.86555E-02	1.02397E-03	-	-	-	-	-	-
2	2.78359E-02	3.72829E-04	9.82942E-06	4.02223E-01	1.47045E-02	2.46630E-04	2.11	2.41	3.26	0.94	1.68	2.47
3	7.55641E-03	5.48334E-05	7.07650E-07	2.04831E-01	3.98353E-03	3.23836E-05	2.07	3.04	4.17	1.07	2.07	3.22
4	1.85386E-03	6.64563E-06	4.16422E-08	1.00781E-01	9.73086E-04	3.81810E-06	2.09	3.14	4.21	1.05	2.10	3.18
5	4.62815E-04	8.10008E-07	2.45361E-09	4.99249E-02	2.39407E-04	4.57147E-07	1.95	2.95	3.98	0.99	1.97	2.98

Table 5: Absolute solution errors for the Poisson's equation with Dirichlet boundary conditions in L^2 and H^1 norms for Ω_a.

Mesh#	$\|e_h\|_{L^2(\Omega_a)}$			$\|e_h\|_{H^1(\Omega_a)}$			Convergence Rate					
							L^2			H^1		
	$p=1$	2	3	1	2	3	1	2	3	1	2	3
1	3.37815E-02	1.79754E-03	9.43075E-05	6.40207E-01	4.12065E-02	9.46073E-04	-	-	-	-	-	-
2	1.21347E-02	4.09281E-04	1.12644E-05	4.00102E-01	1.53434E-02	2.40968E-04	1.78	2.57	3.69	0.82	1.72	2.38
3	3.06093E-03	5.71314E-05	7.70780E-07	2.04377E-01	4.05831E-03	3.18651E-05	2.18	3.12	4.25	1.06	2.11	3.21
4	7.46961E-04	6.82957E-06	4.71858E-08	1.00724E-01	9.83748E-04	3.77874E-06	2.10	3.16	4.15	1.05	2.11	3.17
5	1.81243E-04	8.29064E-07	3.45483E-09	4.99173E-02	2.40787E-04	4.54540E-07	1.99	2.96	3.67	0.99	1.98	2.97

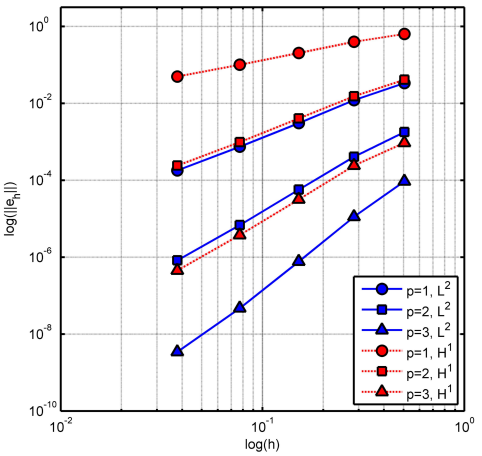

Figure 13: Absolute solution errors for the Poisson's equation with Dirichlet boundary conditions in L^2 and H^1 norms for Ω_a.

3.4 Crack-tip fields in gradient enhanced elasticity

The following set of equations for gradient enhanced stress (σ) fields for crack-tips appears in [Isaksson and Hägglund (2013)],

$$\sigma_{ij} - c^2 \Delta \sigma_{ij} = \frac{K_I}{\sqrt{2\pi r}} f_{ij}(\theta), \quad i,j \in \{1,2\} \text{ in } \Omega. \tag{7}$$

The domain of interest is $\Omega_b = [-0.5, 0.5]^2$. A crack exists along the negative x-axis. K_I is the linear elastic fracture mechanics (LEFM) mode I stress intensity factor, $\theta = \tan^{-1}(y/x)$ and $r = \sqrt{x^2+y^2}$. The analytical solutions for Eq. (7) with angular functions $f_{11}(\theta) = \frac{3}{4}\cos\left(\frac{\theta}{2}\right) + \frac{1}{4}\cos\left(\frac{5\theta}{2}\right)$, $f_{22}(\theta) = \frac{5}{4}\cos\left(\frac{\theta}{2}\right) - \frac{1}{4}\cos\left(\frac{5\theta}{2}\right)$ and $f_{12}(\theta) = \frac{-1}{4}\sin\left(\frac{\theta}{2}\right) + \frac{1}{4}\sin\left(\frac{5\theta}{2}\right)$ are reported in [Isaksson and Hägglund (2013)] as,

$$\sigma_{11} = \frac{K_I}{\sqrt{2\pi r}}\left[\frac{3}{4}\cos\left(\frac{\theta}{2}\right)\left[1-e^{-r/c}\right] + \frac{1}{4}\cos\left(\frac{5\theta}{2}\right)\left[1-6\left(\frac{c}{r}\right)^2 + 2e^{-r/c}\left(3\left(\frac{c}{r}\right)^2 + 3\left(\frac{c}{r}\right)+1\right)\right]\right], \tag{8}$$

$$\sigma_{22} = \frac{K_I}{\sqrt{2\pi r}}\left[\frac{5}{4}\cos\left(\frac{\theta}{2}\right)\left[1-e^{-r/c}\right] - \frac{1}{4}\cos\left(\frac{5\theta}{2}\right)\left[1-6\left(\frac{c}{r}\right)^2 + 2e^{-r/c}\left(3\left(\frac{c}{r}\right)^2 + 3\left(\frac{c}{r}\right)+1\right)\right]\right] \tag{9}$$

$$\sigma_{12}=\frac{K_I}{\sqrt{2\pi r}}\left[\frac{-1}{4}\sin\left(\frac{\theta}{2}\right)\left[1-e^{-r/c}\right]+\frac{1}{4}\sin\left(\frac{5\theta}{2}\right)\left[1-6\left(\frac{c}{r}\right)^2+2e^{-r/c}\left(3\left(\frac{c}{r}\right)^2+3\left(\frac{c}{r}\right)+1\right)\right]\right]. \tag{10}$$

For solving Eq. (7), K_I is taken to be unity and $c = 0.25/1.0951$ [Isaksson and Hägglund (2013)]. The crack is treated as an external boundary for the construction of shape functions. Consequently, nodes are duplicated along the crack. Dirichlet conditions are imposed via the penalty method on $\partial\Omega$ and along the crack using Eq. (8-10). Similar to the Poisson's problem, the penalty factor is taken to be $10^3 h_m^{-p}$ [Fernández-Méndez and Huerta (2004)]. The quadrature rules are identical to the ones employed for the pure Neumann problem, except that a 2 point Gauss quadrature rule is used for numerical integration of boundary integrals for $p=1$. The computed stress fields $\boldsymbol{\sigma}$ are normalized to $\bar{\boldsymbol{\sigma}} := \boldsymbol{\sigma}\,(K_I/\sqrt{c})^{-1}$. The details of the triangulation of Ω_b are summarized in Table 6. Fig. 14 shows the contour plots for computed stress fields upon h refinement for $p = 1$. The bottom row shows the actual solution. Observe the sharpening of contours as the refinement progresses. Similar comments are valid for Fig. 15 where the contour plots for the computed stress fields upon p refinement are shown for Mesh# 1 (Table 6).

Table 6: Domain discretization details of $\Omega_b = [-0.5, 0.5]^2$ for the crack-tip problem.

Mesh#	h	$\lvert V_{\mathrm{D}}\rvert$	$\lvert E_{\mathrm{D}}\rvert$	$\lvert T_{\mathrm{D}}\rvert$	$N(p=1)$	$N(p=2)$	$N(p=3)$
1	0.3156396311877990	30	71	42	30	101	214
2	0.1507447555965090	98	259	162	98	357	778
3	0.0794522561510295	337	944	608	337	1281	2833
4	0.0420821471632756	1268	3673	2406	1268	4941	11020

4 Conclusion

Using simplex splines as kernels, the current work is probably the first attempt at a consistent and rigorous development of a hybrid discretization scheme that puts forth a well charted knotset generation permitting singularity-free evaluation of the shape functions everywhere in the domain. This in itself is a substantial improvement over its predecessor, the DMS-FEM, where the moment matrix invertibility was not guaranteed at element boundaries whilst keeping the degree of the (DMS) spline and the polynomial reproduction order the same. Another implication is the reduction of the number of degrees of freedom per field variable in the proposed method vis-à-vis the DMS-FEM. Numerical evidence also suggests that the

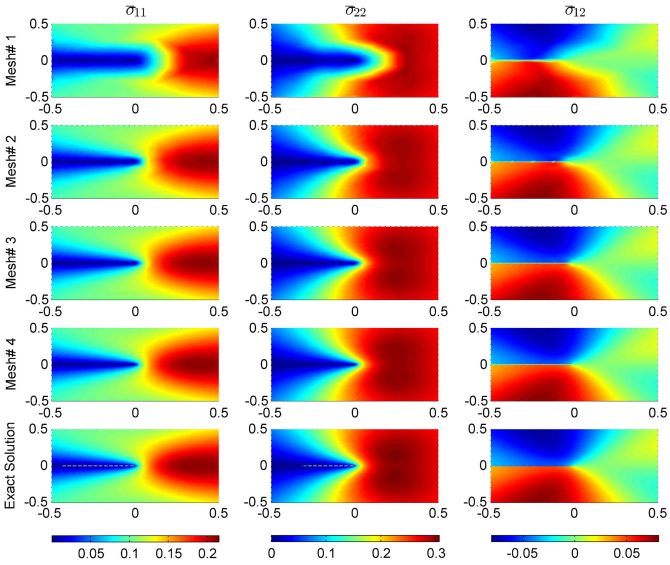

Figure 14: Computed normalized stress fields for $p = 1$ upon h-refinement. The last row shows the exact solution. Observe sharpening of contours on mesh refinement.

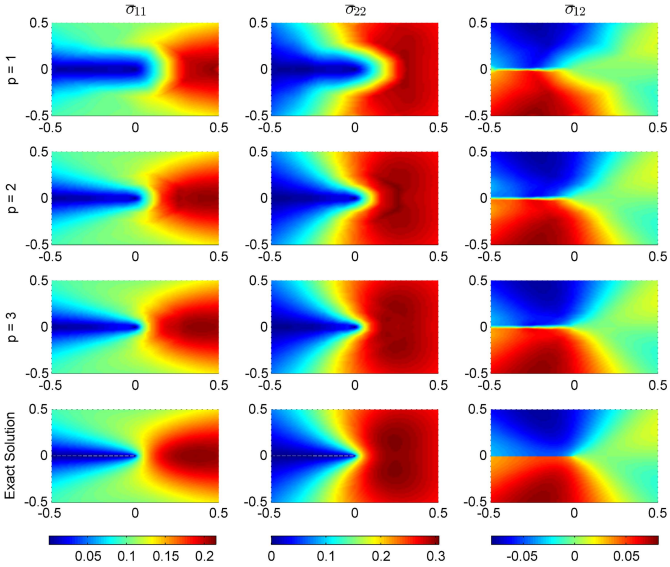

Figure 15: Computed normalized stress fields on Mesh# 1 (Table 6) upon p-refinement. The last row shows the exact solution. Observe sharpening of contours on refinement.

proposed method could offer accurate evaluations of the integrals appearing in the weak forms through lower order quadrature rules. Accurate numerical integration of the weak forms is also aided by a desirable feature of the shape functions, which is the near alignment of the supports (and their intersections) with the triangular domain discretization that doubles as the integration grid. The optimal continuity of the simplex spline kernels is passed on to the approximation space via the polynomial reproduction procedure, even while using conventional FEM-like domain discretization based on Delaunay triangulation. Near optimal convergence rates were obtained for the approximation of standard non-polynomial functions. PDE test cases with pure Neumann and Dirichlet boundary conditions also portray similar convergence rates. Implementation for a gradient enhanced stress field formulation around a crack-tip is also presented.

Future work would include investigations of dependence of approximation properties of the method on knot length variations. Similar investigations for BVPs and conditioning of moment and stiffness matrices also need to be carried out. An important issue which will have to be considered here would be the accuracy of quadrature. Suitable integration routines tailored for the polygonal supports could lead to exact integration. Another promising variant would be to develop a suitable Petrov-Galerkin framework e.g. MLPG [Atluri and Zhu (1998a); Atluri and Zhu (1998b); Atluri and Zhu (2000); Tang, Shen, and Atluri (2003)] for the proposed method. The method can be extended to 3D via either a tensor product approach using NURBS or using tetrahedral discretizations akin to the DMS-FEM. Application wise, the method is currently being applied to a wider class of problems including material and geometric nonlinearity, rate-dependent (or otherwise) plasticity, visco-damage and those with length-scale dependence. Finally, a rigorous mathematical framework needs to be given to the method whilst estimating a-priori errors.

APPENDIX A: Definitions and Properties of simplex splines

Let $W = \{\boldsymbol{x}_i\}_{i=0}^{k}$ be a finite set of points in R^d. The convex hull of W denoted by $[W]$ is the set of all convex combinations of points in W defined as $[W] := \left\{ \sum_{i=0}^{k} \lambda_i \boldsymbol{x}_i : \lambda_i \in \mathrm{R}_0^+, \sum_{i=0}^{k} \lambda_i = 1 \right\}$. W is affinely independent if $\{\boldsymbol{x}_i - \boldsymbol{x}_0\}_{i=1}^{k}$ is a linearly independent set or $\dim\left(span\left(\{\boldsymbol{x}_i - \boldsymbol{x}_0\}_{i=1}^{k}\right)\right) = k$. Equivalently, the points in W do not lie on a $k-1$- dimensional hyperplane. A nonempty set $\Delta \subset \mathrm{R}^d$ is a simplex iff $\Delta = [W]$ for W affinely independent. The points in W are the vertices of the simplex. The dimension of a simplex is defined as $\dim(\Delta) := |W| - 1$. A k-simplex is a simplex of dimension k and is denoted by Δ_k. A 0-simplex is a point, a

1-simplex is an interval, a 2-simplex is a triangle, a 3-simplex is a tetrahedron and so on (by convention $\Delta_{-1} := \emptyset$). An n-face of a k-simplex for $n \in J_k^0$ is defined as any n-simplex whose vertices coincide with the vertices of the k-simplex. Denote by $\Delta^{(n)}$ the set of n-faces of the simplex $\Delta$of dimension k (see Fig. A.1). Clearly, $\left|\Delta^{(n)}\right| = {}^{k+1}C_{n+1}$.

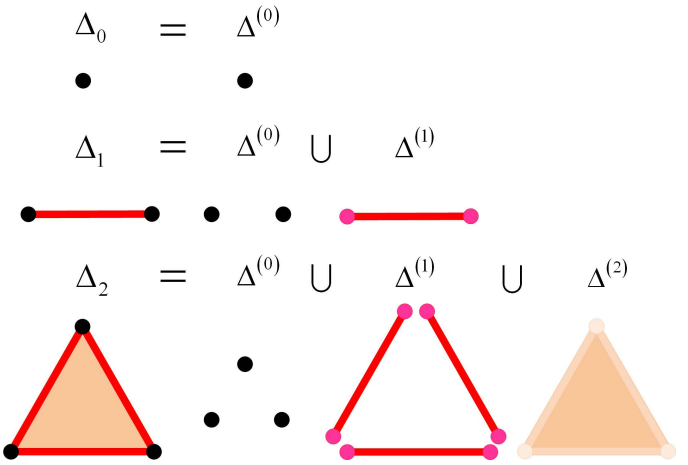

Figure A.1: Simplices and their decomposition into faces.

The determinant of points in $W = \{\boldsymbol{x}_i\}_{i=0}^d$ is defined as

$$D(W) := \det \begin{pmatrix} 1 & \cdots & 1 & \cdots & 1 \\ \boldsymbol{x}_0 & \cdots & \boldsymbol{x}_j & \cdots & \boldsymbol{x}_d \end{pmatrix}.$$

The volume of a d-simplex is given by $vol_d(\Delta_d) = |D(W)|/d!$. A degenerate simplex has zero volume. The standard d-simplex $\hat{\Delta}_d$ is the simplex with vertices $\{e_i\}_{i=1}^{d+1}$, the set of canonical basis vectors of R^{d+1}. The jth barycentric determinant of $\boldsymbol{x} \in \mathrm{R}^d$ for $j \in J_d^0$ with respect to W is defined as, $D_j(W|\boldsymbol{x}) := D(W[\boldsymbol{x}_j/\boldsymbol{x}])$ with $W[\boldsymbol{x}_j/\boldsymbol{x}]$ denoting the set W in which the jth element $\boldsymbol{x}_j$ is replaced by $\boldsymbol{x}$. Let $W = \{\boldsymbol{x}_i\}_{i=0}^d \subset \mathrm{R}^d$ be affinely independent, then the jth barycentric coordinate of $\boldsymbol{x} \in \mathrm{R}^d$ with respect to W is defined as $\lambda_j(W|\boldsymbol{x}) := D_j(W|\boldsymbol{x})/D(W)$ for $j \in J_d^0$ (see Fig. A.2).

Thus, the barycentric coordinates of $\boldsymbol{x}$ with respect to W are the unique solutions to the set of equations $\sum_{j=0}^{d} \lambda_j(W|\boldsymbol{x}) = 1$ and $\sum_{j=0}^{d} \lambda_j(W|\boldsymbol{x})\boldsymbol{x}_j = \boldsymbol{x}$. In addition to forming a partition of unity (i.e. the former equation), the barycentric coordinates are also interpolating and satisfy the following Kronecker delta property viz., $\lambda_j(W|\boldsymbol{x}_i) =$

δ_{ij}. Also, $\boldsymbol{x} \in [W]$ ($([W])^{\circ}$) iff all its barycentric coordinates are non-negative i.e. $\lambda_j(W|\boldsymbol{x}) \geq 0$ (positive i.e. $\lambda_j(W|\boldsymbol{x}) > 0$). In other words, if $\Delta := [W]$, then the sign of $\lambda_j(W|\boldsymbol{x})$ reveals the position of $\boldsymbol{x}$ relative to the hyperplane containing the $d-1$-face of Δ opposite vertex x_j. Specifically, $\lambda_j(W|\boldsymbol{x}) = 0, > 0$ and < 0 whenever $\boldsymbol{x}$ lies on the hyperplane, on the side of the hyperplane containing $\boldsymbol{x}_j$ and on the opposite side of the hyperplane from $\boldsymbol{x}_j$ respectively. The signature of $\boldsymbol{x}$ relative to Δ is defined by $\Sigma(W|\boldsymbol{x}) := (sgn\lambda_0(W|\boldsymbol{x}), \ldots, sgn\lambda_d(W|\boldsymbol{x}))$ with sgn being the usual sign function. For $d = 2$ and 3, the barycentric coordinates are also referred to as the area and volume coordinates respectively. If $W \subset \mathrm{R}^d$ with $|W| = k \geq d+1$, then the following two assertions are equivalent [Hakopian (1982)]: (i) $vol_d([W]) \neq 0$ (ii) $\exists$ a set of indices $\{i_j\}_{j=0}^{d} \subset J_k^0$ such that $\{\boldsymbol{x}_{i_j}\}_{j=0}^{d}$ is affinely independent. The set W is (or the points in W are) r-degenerate if r is the smallest positive integer such that every subset of $d+r$ points in W does not lie on a $d-1$-dimensional hyperplane [Hakopian (1982)]. If every subset of $d+1$ points in W does not lie on a $d-1$-dimensional hyperplane (or they form a d-simplex) then W is in general position.

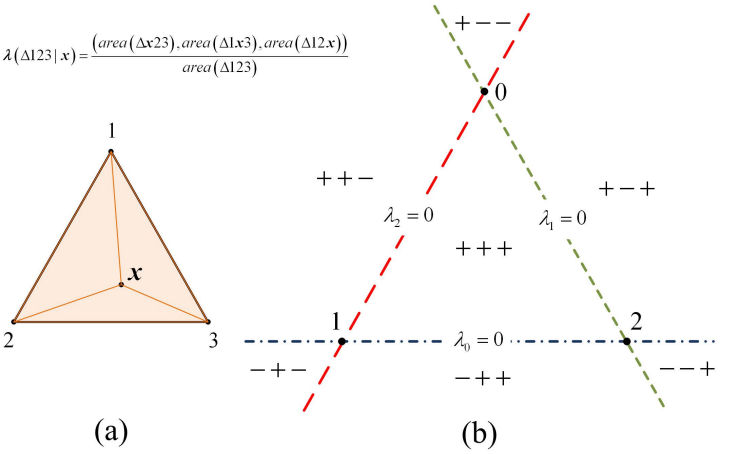

Figure A.2: (a) Definition of barycentric coordinates and (b) their signature on the partition of R^2.

Definition A.1. *(d-variate p-degree simplex spline) Let* $K = \{\boldsymbol{x}_i\}_{i=0}^{k} \subset \mathrm{R}^d, k = d+p$ *be an ordered set of points called the knotset with* $vol_d([K]) > 0$. *The d-variate p-degree simplex spline* $M(\cdot|K)$ *is defined implicitly by the identity* [Dahmen, Micchelli, and Seidel (1992)], $\int_{\mathrm{R}^d} f(\boldsymbol{x}) M(\boldsymbol{x}|K)\, dx_1 \ldots dx_d = p! \int_{\Delta^k} f\left(\sum_{i=0}^{k} \tau_i \boldsymbol{x}_i\right) d\tau_1 \ldots d\tau_k$, $\forall f \in C(\mathrm{R}^d)$, *where* $\hat{\Delta}_k$ *is the standard k-simplex.*

(Although here $k \geq d$, the above equation is valid even for $k < d$ where $M(\cdot|K)$ is interpreted as a distribution on $C_0^{\infty}\left(\mathrm{R}^d\right)$ [Micchelli (1980)].). The elements of K are the *knots* of the simplex spline $M(\boldsymbol{x}|K)$. A geometric interpretation of the d-variate 0-degree simplex is given for any K in general position [Dahmen, Micchelli, and Seidel (1992)],

$$M(\boldsymbol{x}|K) = \chi_{[K]} |D(K)|^{-1}, \ |K| = d+1 \tag{A.1}$$

which is just a normalization of the characteristic function of $[K]$. When the degree of the spline is $k-d = p > 0$, the following recursive formula holds [Dahmen, Micchelli, and Seidel (1992)],

$$M(\boldsymbol{x}|K) = \sum_{i=0}^{d} \lambda_i(U|\boldsymbol{x}) M(\boldsymbol{x}|K \setminus \{\boldsymbol{y}_i\}), \ |K| > d+1, \quad a.e.\ \boldsymbol{x} \in \mathrm{R}^d. \tag{A.2}$$

Therefore, a p-degree ($p > 0$) simplex spline is a combination of $d+1$ number of $p-1$-degree simplex splines. Although $U = \{\boldsymbol{y}_i\}_{i=0}^{d} \subset K$ (called a split set for K) can be any arbitrary subset of $d+1$ points of K with $vol_d([U]) > 0$, it is always possible to choose U such that $\boldsymbol{x} \in U$. Thus, $\lambda_i(U|\boldsymbol{x}) \geq 0$, $i \in J_o^d$ making Eq. (A.2) a convex combination, a property that gives stable numerical routines for calculating $M(\boldsymbol{x}|K)$ (see Fig. A.5). Some important properties of simplex splines are given next.

Property A.2. *(Finite support)* $\operatorname{supp} M(\cdot|K) = [K]$. *Further, if the knots are in general position, then the support is minimal in the sense of* [Dahmen and Micchelli (1983)].

Property A.3. *(Positivity)* $M(\cdot|K) > 0$ on $[K]^{\circ}$ [Dahmen and Micchelli (1983)].

A collection of $d-1$ dimensional sets in R^d is denoted by Γ. Any region in R^d not intersected by any element of Γ is denoted by $\bar{D}$. Define $\pi_{p,d}(\Gamma) := \left\{f : f|_{\bar{D}} \in \pi_{p,d}\right\}$. Any $\rho \in \Gamma$ is a *cut region* for f if $f \in \pi_{p,d}$ only in the region of the neighborhood of some point of ρ that lies on each side of ρ *i.e.* $f \notin \pi_{p,d}$ in the entire neighborhood. The set of cut regions of f is denoted by $\Gamma(f)$. Further, if $f \in \pi_{p,d}(\Gamma)$ then $\Gamma(f) \subset \Gamma$. Regions in R^d that are bounded but not intersected by $\Gamma(f)$ is the *p-region* for f denoted by $\Pi(f)$ (see Fig. A.3). The cut region of $M(\cdot|K)$ is $\Gamma(M(\cdot|K)) = \left\{\left[\left\{\boldsymbol{x}_{i_j}\right\}_{j=0}^{d-1}\right] : 0 \leq i_0 \leq \ldots \leq i_{d-1} \leq k\right\}$ *i.e.* the set of all $d-1$ simplices made by subsets of d points of K and the p-region of $M(\cdot|K)$ is $\Pi(M(\cdot|K)) = [K] \setminus \Gamma(M(\cdot|K))$ [Dahmen and Micchelli (1983)].

Property A.4. *(Polynomial degree)* $M(\cdot|K)$ *is a piecewise polynomial function of degree* $\leq p$. *More precisely,* $M(\cdot|K)$ *agrees with a polynomial of degree* $\leq p$ *on its p-region* [Micchelli (1980)].

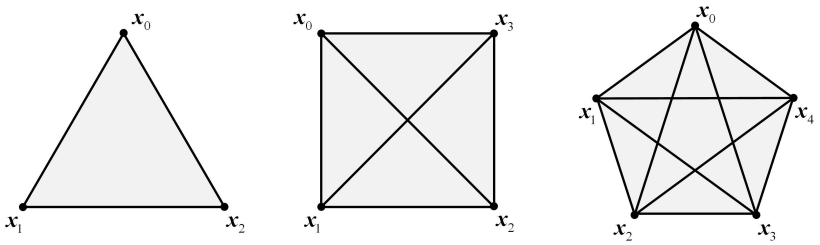

Figure A.3: Knotsets (black dots), cut region (black lines), p-region (grey) for simplex splines of degree (a) 0, (b) 1 and (c) 3 respectively.

Thus, in its p-region, $M(\cdot|K)$ belongs to $C^{\infty}(\Pi(M(\cdot|K)))$. The complete characterization of the continuity of a simplex spline is done globally (over R^d) and locally (over $\Gamma(M(\cdot|K))$). Assume K to be r-degenerate with $r \leq k-d+1$ *i.e.* $vol_d([K]) > 0$ and let H_ρ be the $d-1$-dimensional hyperplane spanned by $\rho \in \Gamma(M(\cdot|K))$. For $\boldsymbol{x} \in \left[K \cap H_\rho\right]^\circ$ define $l := k - \left|K \cap H_\rho\right| - 1$. It is easy to verify that $\left|K \cap H_\rho\right| \leq d+r-1$. Let $C^{-1} \backslash C^0 = \left\{f : f \notin C^0\right\}$ and $D_y^f := \sum_{i=1}^d y_i \frac{\partial f}{\partial x_i}$ be the directional derivative of f along $\boldsymbol{y}$.

Property A.5. *(i) (Global Continuity) Provided that the knots are r-degenerate,* $M(\cdot|K) \in C^{p-r}\left(\mathrm{R}^d\right)$. *Further,* $M(\cdot|K) \in C^{p-r}\left(\mathrm{R}^d\right) \backslash C^{p-r+1}\left(\mathrm{R}^d\right)$ *i.e. the continuity is the best possible* [Hakopian (1982)]. *(ii) (Local Continuity) Let* $\boldsymbol{x} \in \left[K \cap H_\rho\right]^\circ$ relative to H_ρ and $\boldsymbol{y} \perp H_\rho$ then $0 < \lim_{t \to 0^+} \left|D_y^{l+1} M(\boldsymbol{x}+t\boldsymbol{y}|K) - D_y^{l+1} M(\boldsymbol{x}-t\boldsymbol{y}|K)\right| < \infty$ [Dahmen and Micchelli (1983)].

Thus, the global continuity of the d-variate p-degree simplex spline whose knots are in general position is *optimal i.e.* belonging to $C^{p-1}\left(\mathrm{R}^d\right)$. It is called optimal because for a compactly supported piecewise polynomial function f of order p, if $f \in C^p\left(\mathrm{R}^d\right)$ then $f \in \pi_{p,d}\left(\mathrm{R}^d\right)$ *i.e.* f is a polynomial and thus with infinite support, a contradiction.

Property A.6. *(Affine transformation) For* $K = \{\boldsymbol{x}_i\}_{i=0}^k$ *let* $K + \boldsymbol{y} := \{\boldsymbol{x}_i + \boldsymbol{y}\}_{i=0}^k, \boldsymbol{y} \in \mathrm{R}^d$ *and* $\boldsymbol{A}$ *be any nonsingular* $n \times n$ *matrix, then* $M(\boldsymbol{A}\boldsymbol{x}+\boldsymbol{y}|K+\boldsymbol{y}) = M(\boldsymbol{x}|K)/\det \boldsymbol{A}$ [Hakopian (1982)].

The recurrence relation given in Eq. (A.2) is defined for *a.e.* $\boldsymbol{x} \in \mathrm{R}^d$. Specifically, if $\boldsymbol{x} \notin \Gamma(M(\boldsymbol{x}|K))$then the relation holds else the equation may not hold true unless the characteristic function in Eq. (A.1) is appropriately modified. The union of boundaries of supports of all possible 0-degree splines produced by Eq. (A.1) gives $\Gamma(M(\boldsymbol{x}|K))$. To avoid ambiguity of definition of the simplex spline on $\Gamma(M(\boldsymbol{x}|K))$,

the characteristic function in Eq. (A.1) is modified to use $[K)$, the half-open convex hull of K (defined below) rather than $[K]$ [Seidel (1992)]. Consequent to this modification, the new expression for the d-variate simplex spline is written as,

$$M(\boldsymbol{x}|K) = \begin{cases} \chi_{[K)} |D(K)|^{-1} & |K| = d+1 \\ \sum_{i=0}^{d} \lambda_i(U|\boldsymbol{x}) M(\boldsymbol{x}|K\backslash\{\boldsymbol{y}_i\}) & |K| > d+1 \quad \boldsymbol{x} \in \mathrm{R}^d \end{cases} \tag{A.3}$$

Definition A.7. *(Half-open convex hull) Let $W \subset \mathrm{R}^d$ and $\{e_i\}_{i=0}^{d-1}$ be the canonical basis of R^d, then the half-open convex hull $[W)$ of W is defined as, $\boldsymbol{x} \in [W)$ iff $\exists \eta_0, \ldots, \eta_{d-1} > 0$ such that $\boldsymbol{x} + \left\{ \sum_{i=0}^{d-1} \varepsilon_i \eta_i e_i \right\} \in [W], \forall 0 \le \varepsilon_{d-1} \le \ldots \le \varepsilon_1 \le \varepsilon_0, 0 < \varepsilon_0 < 1$* [Franssen (1995)]. *(See Fig. A.4)*

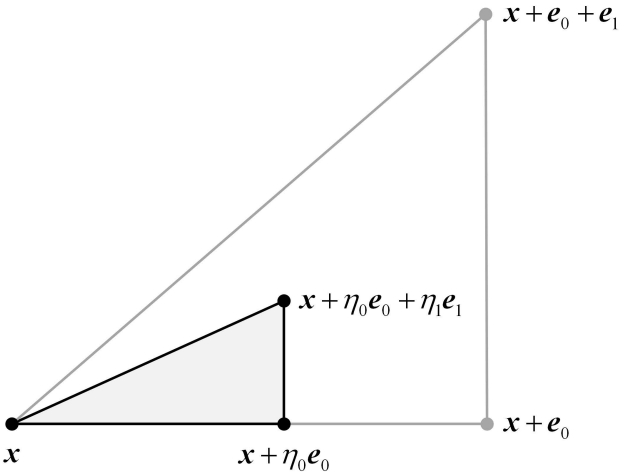

Figure A.4: The 2-simplex (grey) added to $\boldsymbol{x}$ in Definition A.7 of half-open convex hull for R^2. (adapted from [Franssen (1995)].)

Being a generalization of the half-open domain in R, the half-open convex hulls of the knotsets appearing in the constant spline creation in Eq. (A.3) assign each point on $\Gamma(M(\boldsymbol{x}|K))$ to exactly one the knotsets.

A.1 Sample evaluation routine for a bivariate quadratic simplex spline

In Fig. A.5, the knotset $K_I = \{\boldsymbol{x}_i\}_{i=0}^{4}$ is in general position (*i.e.* every subset of 3 points in K forms a 2-simplex). Thus the resultant spline $M(\cdot|K)$ is of degree 2 (*i.e.* quadratic) depicted by its support in Level 2. The diagram shows the evaluation of

$M(\boldsymbol{x}|K)$ in three levels (for a p-degree simplex spline $p+1$ levels will be present). Choose the split set as $U_I = \{\boldsymbol{x}_0, \boldsymbol{x}_2, \boldsymbol{x}_3\}$ for the first unfolding of the recursive procedure in Eq. (A.3). U_I is chosen so as to get the barycentric coordinates of $\boldsymbol{x}$ with respect to U_I as non-negative. The same is not true for an alternative split set (say, $\{\boldsymbol{x}_0, \boldsymbol{x}_1, \boldsymbol{x}_4\}$) even though it is also a correct choice resulting in the same spline. In practice, such a decision may be taken by computing the signature $\Sigma(U_I|\boldsymbol{x})$. Consequently, Eq. (A.3) at this unfolding becomes a convex combination of three 1- degree (*i.e.* linear) simplex splines. Their respective knotsets are depicted in Level 1 *viz.*, $K_a = K_I \setminus \{\boldsymbol{x}_0\}$, $K_b = K_I \setminus \{\boldsymbol{x}_2\}$ and $K_c = K_I \setminus \{\boldsymbol{x}_3\}$ formed by removing three points one at a time from K_I. The choice of split sets $U_a = \{\boldsymbol{x}_1, \boldsymbol{x}_2, \boldsymbol{x}_4\}$, $U_b = \{\boldsymbol{x}_0, \boldsymbol{x}_1, \boldsymbol{x}_3\}$ and $U_c = \{\boldsymbol{x}_0, \boldsymbol{x}_2, \boldsymbol{x}_4\}$ for the second unfolding of the recursive procedure is such that the barycentric coordinates of $\boldsymbol{x}$ with respect to U_a, U_b and U_c are non-negative. Level 0 depicts the seven knotsets of three points each (*i.e.* each resulting in a 0-degree simplex spline) to be used in the final stage of the recursive procedure. They are formed by removing three points at a time from the respective split set of Level 1. Thus, K_a gives rise to $K_i = K_a \setminus \{\boldsymbol{x}_1\}$, $K_{ii} = K_a \setminus \{\boldsymbol{x}_4\}$ and $K_{iii} = K_a \setminus \{\boldsymbol{x}_2\}$. K_b gives rise to $K_{iii} = K_b \setminus \{\boldsymbol{x}_0\}$, $K_{iv} = K_b \setminus \{\boldsymbol{x}_1\}$ and $K_v = K_b \setminus \{\boldsymbol{x}_3\}$. And K_c gives rise to $K_v = K_c \setminus \{\boldsymbol{x}_2\}$, $K_{vi} = K_c \setminus \{\boldsymbol{x}_4\}$ and $K_{vii} = K_c \setminus \{\boldsymbol{x}_0\}$.

It may be noted that a blind evaluation of every constant simplex spline required at Level 0 would result in $3^{p=2} = 9$ evaluations, but in practice two of them are same *viz.*, K_{iii} and K_v, although they originate from different routes. For an efficient fast algorithm and associated data structure to select split sets and reusing partial evaluations refer [Franssen, Veltkamp, and Wesselink (2000)].

APPENDIX B: Definition and properties of triangulations and d-simplices of type p

For a n-simplex Δ, define the relation $\prec$ in the set $\bigcup_{i=-1}^{n} \Delta^{(i)}$ as $s_1 \prec s_2$ iff s_1 is a face of s_2. The set of *proper faces* of Δ is given by $\bigcup_{i=-1}^{n-1} \Delta^{(i)}$. A finite set S of simplices is called a *simplical complex*, (i) if $s_1, s_2 \in \mathrm{S}$ then either $s_1 \cap s_2 = \emptyset$ or $s_1 \cap s_2 \prec s_i$, $i \in \{1,2\}$, and (ii) if $s \in \mathrm{S}$ and $s' \prec s$ then $s' \in \mathrm{S}$. The *n-dimensional skeleton* of S is the set of n-simplices in S and is denoted by$\mathrm{S}^{(n)}$. The *dimension of* S is defined as $\dim(\mathrm{S}) := \max\{\dim(s) : s \in \mathrm{S}\}$. The *geometric realization* of S is $[\![\mathrm{S}]\!] := \bigcup \mathrm{S}$. The dimension of S is assumed to be d to avoid simplical complexes of lower dimensions in R^d *e.g.* a triangular mesh embedded in R^3. Also, assume $[\![\mathrm{S}]\!]$ is connected to avoid configurations with isolated simplices.

Definition B.1. *(Triangulation) Let $P \subset \mathrm{R}^d$ be a finite point set then a simplical complex* T *is a triangulation of P if* $[P] = [\![\mathrm{T}]\!]$ *and* $P = \mathrm{T}^{(0)}$ [Moszynska (2006)].

P is the set of *forming points* of T. (Triangulations are also defined for sets other

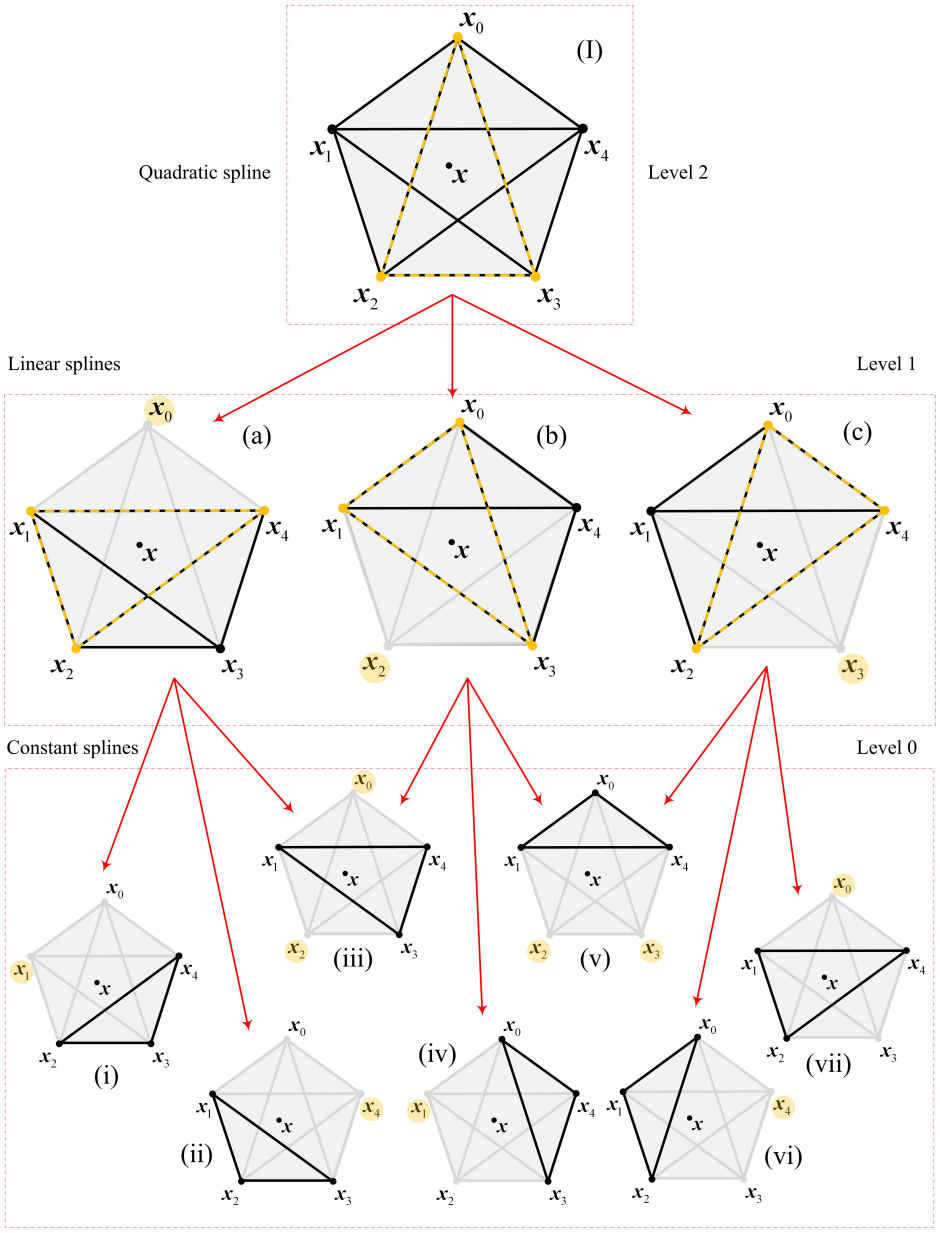

Figure A.5: Recursive evaluation of a quadratic simplex spline in terms of unfolding of recursive Eq. (A.3). Split sets are shown by yellow-black dotted lines.

than point sets *e.g.* a triangulation of a closed region $Q \subset \mathrm{R}^d$ is a simplical complex T such that$Q = [\![\mathrm{T}]\!]$ in which case, Q is *polyhedron*. Also, a triangulation of any compact set $Q' \subset \mathrm{R}^d$ is possible in the sense that Q' can be approximated by a sequence of polyhedra. Similarly, triangulation of domains with holes is also possible.) Distinct elements of the triangulation intersect only on their proper faces *i.e.* if $s_1, s_2 \in \mathrm{T}$, $s_1 \neq s_2$ then $s_1^\circ \cap s_2^\circ = \emptyset$. Further, the elements of $\mathrm{T}^{(d)}$ are all assumed to be of anticlockwise orientation *i.e.* $vol_d(\Delta) > 0, \Delta \in \mathrm{T}^{(d)}$. Specifically, define the set of *vertices, facets* and *d-simplices of* T as $V_\mathrm{T} := \mathrm{T}^{(0)}$, $E_\mathrm{T} := \mathrm{T}^{(d-1)}$ and $T_\mathrm{T} := \mathrm{T}^{(d)}$ respectively. Clearly, $|V_\mathrm{T}| = |P|$. The boundary of the triangulation is denoted by $\partial\mathrm{T} := \partial [\![\mathrm{T}]\!]$. Any $v \in V_\mathrm{T}$ is either an *interior* or a *boundary* vertex*i.e.* either $v \cap \partial\mathrm{T} = \emptyset$ or $\neq \emptyset$ respectively. Their sets are denoted by $V_\mathrm{T}^I \subset V_\mathrm{T}$ and $V_\mathrm{T}^B = V_\mathrm{T} \backslash V_\mathrm{T}^I$ respectively. Any $e \in E_\mathrm{T}$ is either a *boundary* or an *interior facet i.e.* $vol_{d-1}(e \cap \partial\mathrm{T}) \neq 0$ or $= 0$ respectively. Their sets are denoted by $E_\mathrm{T}^I \subset E_\mathrm{T}$ and $E_\mathrm{T}^B = E_\mathrm{T} \backslash E_\mathrm{T}^I$ respectively. The *degree of a vertex v* denoted by $\deg(v)$ is defined as the number of facets incident with v. The *F-vector* of T is denoted by $\boldsymbol{f}_\mathrm{T} := \left(f_\mathrm{T}^{-1}, f_\mathrm{T}^0, \ldots, f_\mathrm{T}^d\right)^T$ with $f_\mathrm{T}^n := \left|\mathrm{T}^{(n)}\right|$, $n \in J_d$ (and $f_\mathrm{T}^{-1} = |\{\emptyset\}| = 1$). If $\dim(\mathrm{T}) = 2$ then with $\alpha = \left|V_\mathrm{T}^I\right|$, $\beta = \left|V_\mathrm{T}^B\right|$ $\boldsymbol{f}_\mathrm{T} := (1, \alpha+\beta, 3\alpha+2\beta-3, 2\alpha+\beta-2)^T$ and $\left|E_\mathrm{T}^I\right| = 3\alpha+\beta-3$. The F-vector of a k-simplex is denoted by $\boldsymbol{f}_{\Delta_k}$ with its components $f_{\Delta_k}^{n-1} = {}^{k+1}C_n$, $n \in J_{k+1}^0$.

Since a triangulation for a given forming points is non-unique, an optimal triangulation from the family of all triangulations is the *Delaunay triangulation* [Hjelle and Dæhlen (2006)]. Lets balls with centre $\boldsymbol{x}_0 \in \mathrm{R}^d$ and radius $r \in \mathrm{R}^+$ be represented by $B_r(\boldsymbol{x}_0) = \left\{x \in \mathrm{R}^d : \|\boldsymbol{x} - \boldsymbol{x}_0\|_2 < r\right\}$. Define a $d-1$-*dimensional sphere* as the boundary of a d-dimensional ball *i.e.* $\partial B_r(\boldsymbol{x})$, $\boldsymbol{x} \in \mathrm{R}^d$. A point set is *regular* if no subset of $d+2$ points lie on a common $d-1$-sphere.

Definition B.2. *(Delaunay triangulation) A triangulation* D *of a regular finite set of points $P \subset \mathrm{R}^d$ is a Delaunay triangulation if $\Delta \in T_\mathrm{D}$ then $\exists$ a $d-1$-dimensional sphere Θ called the circumsphere of Δ such that $\Theta(\boldsymbol{x}) = 0, \forall \boldsymbol{x} \in \Delta^{(0)}$ and $\Theta(\boldsymbol{x}) > 0$, $\forall \boldsymbol{x} \in P \backslash \Delta^{(0)}$ [Rajan (1994)].*

The criteria stated in the definition are the *in-sphere* and *empty-sphere* criterion respectively. Elements of T_D are *Delaunay d-simplices*. The important optimality properties of a Delaunay triangulation D of dimension 2 in the family of all triangulations of a forming point set are given next. First, D maximizes the minimum angle in all the triangles in T_D. (But neither is the converse true nor does D necessarily maximize the minimum angle in all the triangles). Second, D minimizes the maximum radius of circumcircles of all the Delaunay triangles. Consequently, D does not contain elongated, poorly shaped and almost degenerate triangles. This has particular relevance for the 2D FEM interpolation error estimate in which the maximum (or in some estimates, the minimum) angle and maximum

circumradius (as a measure of maximum triangle edge length) are parameters. A measure of the roughness of a surface f on Ω is the *Dirichlet functional defined* as $D_\Omega(f) := \int_\Omega \|\nabla f\|_2^2 d\Omega$. $\tilde{f}$ is the piecewise linear interpolating surface of f over $[P]$ defined as $\tilde{f}\big|_{\Delta_i} := \phi_i$, where ϕ_i is the unique piecewise linear interpolation of f over $\Delta_i \in T_\mathrm{D}$ determined by $\varphi_i(\boldsymbol{x}) = f(\boldsymbol{x})$, $\boldsymbol{x} \in \Delta_i^{(0)}$. Third, D minimizes $\sum_{i=1}^{|T_\mathrm{T}|} D_{\Delta_i}(\phi_i)$, the roughness of $\tilde{f}$ on $[P]$. The following optimality properties hold for D of any dimension. The *min-containment sphere* of $\Delta \in T_\mathrm{D}$ is the smallest $d-1$-dimensional sphere containing Δ°. If the circumcentre of Δ lies in Δ° then its min-containment sphere is its circumsphere else it is the circumsphere of one of its facets. Fourth, D minimizes the maximum min-containment radius of all the triangles in T_D. For more information on Delaunay triangulations, refer [Hjelle and Dæhlen (2006); Rajan (1994); Rippa (1990)].

Definition B.3. (*d-simplex of type p*) *Let Δ_d be a d-simplex with the set of vertices $\{\boldsymbol{x}_i\}_{i=0}^d \subset \mathrm{R}^d$. The d-simplex of type $p \in \mathrm{Z}^+$* is $L_p(\Delta_d)$ *and defined as [Ciarlet (1978)],* $L_p(\Delta_d) := \left\{ \boldsymbol{x} = \sum_{i=0}^d \lambda_i \boldsymbol{x}_i : \sum_{i=0}^d \lambda_i = 1, p\lambda_i \in J_p^0, i \in J_d^0 \right\}$.

$L_p(\Delta_d)$ is also referred to as the *principal lattice of order p* of Δ_d [Ciarlet (1978); Chung, Yao (1977)] (see Fig. B.1). It is clear that $L_1(\Delta_d) \neq \Delta_d$ since λ_is are elements of the discrete set $J_1^0 = \{0,1\}$ rather than the continuum R_0^+ as in the definition of Δ_d. It is actually the set of vertices of Δ_d. But for all practical purposes, $L_1(\Delta_d) = \Delta_d$ connotes the above characterization of $L_1(\Delta_d)$ through the vertices of Δ_d. In the context of FEM, a 2-simplex of type 1, 2 and 3 is the stencil of points associated with the *linear (or Courant), quadratic* and *cubic Lagrange triangle* respectively [Ciarlet (1978)]. Similarly, a 3-simplex of type 1, 2 and 3 is the stencil of points associated with the *linear, quadratic* and *cubic tetrahedron* respectively.

Theorem B.4. *(Unique Lagrange interpolation from $\pi_{p,d}(\mathrm{R}^d)$) Any element of $\pi_{p,d}(\mathrm{R}^d)$ is uniquely determined by its evaluations on $L_p(\Delta_d)$ [Ciarlet (1978)].*

In other words, the Lagrange interpolation problem for $L_p(\Delta_d)$ is *poised* in $\pi_{p,d}(\mathrm{R}^d)$ and $|L_p(\Delta_d)| = \dim(\pi_{p,d}(\mathrm{R}^d)) = N_{p,d}$. An element $\Delta \in T_\mathrm{D}$ is a d-simplex of type 1. The characterization of points in Δ such that they are poised in $\pi_{p,d}(\mathrm{R}^d)$ necessitates the construction of $L_p(\Delta)$. The elements of $L_p(\Delta)$ are the *nodes* of Δ. Denote the set of *nodes* in a Delaunay triangulation D by $X_\mathrm{D} := \bigcup_{i=1}^{|T_\mathrm{D}|} L_p(\Delta^i)$, $\Delta^i \in T_\mathrm{D}$. Any $\boldsymbol{x} \in X_\mathrm{D}$ is either an *interior* or a *boundary node* depending on whether $\boldsymbol{x} \cap \partial\mathrm{D} = \emptyset$ or $\neq \emptyset$ respectively. Their sets are denoted by $X_\mathrm{D}^I \subset X_\mathrm{D}$ and $X_\mathrm{D}^B = X_\mathrm{D} \backslash X_\mathrm{D}^I$ respectively. The *local neighborhood* of $\boldsymbol{x} \in X_\mathrm{D}$ is $\aleph(\boldsymbol{x})$ and defined as the set of all elements of T_D that have a non-empty intersection with $\boldsymbol{x}$ i.e. $\aleph(\boldsymbol{x}) := \{\Delta : \Delta \in T_\mathrm{D}, \Delta \cap x \neq \emptyset\}$. Call X_D^n, $n \in J_d^0$ as the set of *n-face proper nodes of* Dconsisting of nodes that lie on an n-face but not on an $n-1$-face of D,

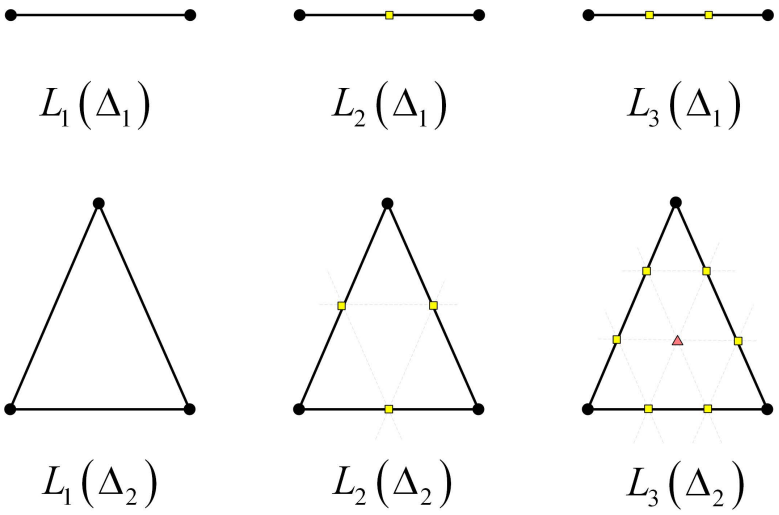

Figure B.1: Principal lattices. Elements of X_{D}^V (black dots), X_{D}^E (yellow squares) and X_{D}^T (rose triangles) in the second row.

i.e. $X_{\mathrm{D}}^n := \left\{\boldsymbol{x} : \boldsymbol{x} \cap \Delta \neq \emptyset, \boldsymbol{x} \in X_{\mathrm{D}}, \Delta \in \mathrm{D}^{(n)}\right\} \setminus \bigcup_{i=0}^{n} X_{\mathrm{D}}^{i-1}$ recursively with $X_{\mathrm{D}}^{-1} := \emptyset$. Consequently, $V_{\mathrm{D}} = X_{\mathrm{D}}^0$. Specifically, define the set of *vertex, facet and interior nodes* as $X_{\mathrm{D}}^V := X_{\mathrm{D}}^0$, $X_{\mathrm{D}}^E := X_{\mathrm{D}}^{d-1}$ and $X_{\mathrm{D}}^T := X_{\mathrm{D}}^d$ respectively. It is easy to verify that the disjoint union $\bigcup_{i=0}^{d} X_{\mathrm{D}}^i = X_{\mathrm{D}}$. Define the P-vector $\boldsymbol{p}_{\mathrm{D}} := \left(p_{\mathrm{D}}^{-1}, p_{\mathrm{D}}^0, \ldots, p_{\mathrm{D}}^d\right)^T$ with $p_{\mathrm{D}}^{n-1} := \left|X_{\mathrm{D}}^{n-1}\right|$, $n \in J_{d+1}^0$ (and $p_{\mathrm{D}}^{-1} = |\emptyset| = 0$) so that $|X_{\mathrm{D}}| = |\boldsymbol{p}_{\mathrm{D}}| =: N$. Finally, the indexing in $X_{\mathrm{D}} := \{\boldsymbol{x}_i\}_{i=1}^N$ is such that $X_{\mathrm{D}}^n = \left\{\boldsymbol{x}_i : i \in \left\{p_{\mathrm{D}}^{n-1} + 1, \ldots, p_{\mathrm{D}}^n\right\}\right\}$.

APPENDIX C: Brief outline of a polynomial reproducing mesh-free method and $\pi_{p,d}$-unisolvence

(This appendix follows the notations and terms used in Section 2.4.) First note that the terms particle, patch, patch diameter, particle density index, nodal parameters and star of nodes in the context of mesh-free particle methods are reminiscent of nodes, element, element size, refinement, nodal values and connectivity respectively in the context of classical FEM. Some definitions are pertinent for the discussions related to any approximation scheme. A scheme $\mathscr{L}_h u = f$ that is consistent with the differential equation $\mathscr{L} u = f$ is *accurate(consistent) of order* p if for any sufficiently smooth function u, $\mathscr{L} u - \mathscr{L}_h u = O(h^p)$ [Belytschko, Krongauz, Dolbow, and Gerlach (1998)]. The approximation scheme is said to possess *p-th order accuracy* and p is called the *order of consistency* of the approximation scheme. For $O(h^p) \to 0$ as $h \to 0$, the necessary requirement is that $p > 0$. Also, consistency

plus stability implies convergence. Higher values of p viz. $p \geq 1$ imply better convergence [Belytschko, Krongauz, Dolbow, and Gerlach (1998)].

Definition C.1 *(Polynomial reproduction/Completeness) The approximation $\tilde{u}(\boldsymbol{x})$ is complete to order p or the set of shape functions Φ_N reproduces polynomials up to order p if it can represent exactly any polynomial up to order p i.e.* $u(\boldsymbol{x}) = \tilde{u}(\boldsymbol{x}) = \sum_{i=1}^{N} u(\boldsymbol{x}_i)\,\varphi_i(\boldsymbol{x}), \forall u \in \pi_{p,2}\left(\bar{\Omega}\right)$ [Belytschko, Krongauz, Dolbow, and Gerlach (1998)].

In the context of convergence analysis of Galerkin methods, p is the *order of consistency* of the shape functions and likewise, $\tilde{u}(\boldsymbol{x})$ and Φ_N are said to possess *p-th order consistency*.

A brief outline of the RKPM is given next. Let $\delta(\cdot)$ represent the Dirac delta distribution and its convolution '$*$' with any $u \in C^0\left(\bar{\Omega}\right)$ is written as

$$u(x) = \delta * u := \int_{\Omega} \delta(x-s)\,u(s)\,ds \;\; \forall x \in \Omega, \tag{C.1}$$

In a numerical implementation of Eq. (C.1), $\delta(\boldsymbol{x})$ is replaced by a finite-valued kernel approximation, $\varepsilon^{-d} w_\varepsilon(\boldsymbol{x})$ with $w_\varepsilon(\boldsymbol{x}) := w(\boldsymbol{x}/\varepsilon)$ and $\varepsilon > 0$ small. The *kernel function w* is also known as the *generating* or *window* function and is a continuous ($C^k(\Omega)$), non-negative, compactly supported function in R^d [Han and Meng (2001)] A measure of supp$w$ is ε called the *dilation parameter* or *smoothing length*. $\varepsilon^{-d} w_\varepsilon(\cdot)$ is more commonly known as a *mollifier*. Applying a *correction function* $C(\boldsymbol{x},\boldsymbol{s}) := \sum_{|\alpha| \leq p} c_{\boldsymbol{\alpha}}(\boldsymbol{x})(\boldsymbol{x}-\boldsymbol{s})^{\boldsymbol{\alpha}} = \boldsymbol{H}^T(\boldsymbol{x}-\boldsymbol{s})\,\boldsymbol{c}(\boldsymbol{x})$ to the kernel allows for $\tilde{u}$ being complete to order p near $\partial\Omega$ [Han and Meng (2001)]. Here, $\boldsymbol{c}(\boldsymbol{x}) \in \mathrm{R}^{N_{p,d}}$ is the vector resulting from the post lexical ordering on $\{c_{\boldsymbol{\alpha}} : |\boldsymbol{\alpha}| \leq p\}$ called the *coefficient functions*. A suitable quadrature rule replaces the integration over Ω in Eq. (C.1) by a summation over the particles $X_N := \{\boldsymbol{x}_i\}_{i=1}^N$

$$\tilde{u}(\boldsymbol{x}) = \sum_{i=1}^{N} \left(\varepsilon_i^{-d} C(\boldsymbol{x},\boldsymbol{x}_i)\, w_i(\boldsymbol{x}-\boldsymbol{x}_i)\, u(\boldsymbol{x}_i)\, \mathrm{V}_i\right), \tag{C.2}$$

where $\{\mathrm{V}_i > 0\}_{i=1}^N$ is the set of *quadrature weights*, $\{\varepsilon_i\}_{i=1}^N$ is the set of dilation parameters and for brevity $w_i := w_{\varepsilon_i}$. The normalizing condition $\int_\Omega w(\boldsymbol{x})\,d\Omega = 1$ which is sometimes prescribed as a property of w may be abandoned due to its absorption in $C(\boldsymbol{x},\boldsymbol{x}_i)$ along with ε_i^{-d} [Han and Meng (2001)]. Thus, Eq. (C.2) may be recast as $\tilde{u}(\boldsymbol{x}) = \sum_{i=1}^{N} u(\boldsymbol{x}_i)\,\phi_i(\boldsymbol{x})$ with the shape function being given by,

$$\varphi_i(\boldsymbol{x}) = w_i(\boldsymbol{x}-\boldsymbol{x}_i)\,\mathrm{V}_i \boldsymbol{H}^T(\boldsymbol{x}-\boldsymbol{x}_i)\,\boldsymbol{c}(\boldsymbol{x}). \tag{C.3}$$

To uniquely solve for $\boldsymbol{c}(\boldsymbol{x})$, N_p equations are required which are supplied by imposing the condition that $\tilde{u}(x)$ is complete to order p in d variables *i.e.*

$$\tilde{u}(\boldsymbol{x}) = \sum_{i=1}^{N} \mathrm{V}_i w_i(\boldsymbol{x}-\boldsymbol{x}_i)\boldsymbol{H}^T(\boldsymbol{x}-\boldsymbol{x}_i)u(\boldsymbol{x}_i)\boldsymbol{c}(\boldsymbol{x}) \;\; \forall u \in \pi_{p,d}(\bar{\Omega}). \tag{C.4}$$

Substituting the *complete shifted Taylor monomial basis* $\left\{(\boldsymbol{x}-\boldsymbol{x}_i)^{\boldsymbol{\alpha}} : |\boldsymbol{\alpha}| \leq p\right\}$ for $u(\boldsymbol{x}_i)$ in Eq. (C.4) results in the linear system of equations written as,

$$\boldsymbol{M}(\boldsymbol{x})\,\boldsymbol{c}(\boldsymbol{x}) = \boldsymbol{H}(0), \tag{C.5}$$

where $\boldsymbol{M}(\boldsymbol{x}) = \sum_{i\in\mathscr{S}(x)} \mathrm{V}_i w_i(\boldsymbol{x}-\boldsymbol{x}_i)\boldsymbol{H}(\boldsymbol{x}-\boldsymbol{x}_i)\boldsymbol{H}^T(\boldsymbol{x}-\boldsymbol{x}_i)$ is the *discrete moment matrix* and the sum over N particles being replaced by just $\Lambda = |\mathscr{S}(\boldsymbol{x})| < N$ particles if the finite pointwise overlap property is satisfied for the set of patches Θ_N. An equation in the system (C.4) is given by $\sum_{|\boldsymbol{\alpha}|\leq p} m_{\boldsymbol{\alpha}+\boldsymbol{\beta}}(\boldsymbol{x})\,c_{\boldsymbol{\alpha}}(\boldsymbol{x}) = \delta_{|\boldsymbol{\beta}|0} \;\; |\boldsymbol{\beta}| \leq p$ where $m_{\boldsymbol{\gamma}}(x) = \sum_{i\in\mathscr{S}(\boldsymbol{x})} \mathrm{V}_i w_i(\boldsymbol{x}-\boldsymbol{x}_i)(\boldsymbol{x}-\boldsymbol{x}_i)^{\boldsymbol{\gamma}}$ is the *discrete moment function*. Ideally $\sum_{i=1}^{N} \mathrm{V}_i \sim vol_d(\Omega)$, but in this work $\mathrm{V}_i = 1$ for $i \in J_N$ is taken. In this case the polynomial reproducing scheme is equivalent to the MLS approximation [Nguyen, Rabczuk, Bordas, and Duflot (2008)]. Further $\mathrm{V}_i = 1$, yields the same result as when V_i is any positive constant *e.g.* $\mathrm{V}_i = vol_d(\Omega)/N$. It may be noted that in the definition of the correction function as well as in the imposition of the polynomial reproduction property in Eq. (C.4), the shifted Taylor monomial basis of $\pi_{p.d}$ was used. Other complete bases of $\pi_{p.d}$ in shifted and/or non-shifted versions may also be employed for the task. The end result (*i.e.* Φ_N) will be the same but via differently conditioned moment matrices. The success of the polynomial reproducing scheme primarily revolves around the solvability of Eq. (C.5) *i.e.* the invertibility of $\boldsymbol{M}(\boldsymbol{x})$ for $\boldsymbol{x} \in \bar{\Omega}$

$\pi_{p,d}$ − unisolvence.

A set $Z \subset \mathrm{R}^d$ is $\pi_{p,d}$-*unisolvent* iff $f \in \pi_{p,d}$ and $f(z) = 0$ for all $z \in Z$ implies $f \equiv 0$. The set $Z = \{z_i\}_{i=1}^{N_{p,d}}$ is $\pi_{p,d}$-unisolvent is equivalent to the fact that Z admits a unique polynomial interpolation in $\pi_{p,d}$ (or Z is poised in $\pi_{p,d}$) *i.e.* for given a set $\{f_i\}_{i=1}^{N_{p,d}}$ there exists a unique polynomial $\pi \in \pi_{p,d}$ such that $\pi(z_i) = f_i$ for all $z_i \in Z$ [Ciarlet and Raviart (1972)]. A necessary and sufficient condition for Z to be $\pi_{p,d}$-unisolvent is that it is not contained in an algebraic curve of degree p. The following theorem appears in different forms and situations in [Han and Meng (2001) Melenk (2005); Zuppa (2003a); Armentano (2001); Zuppa (2003b)].

Theorem C.2. *(Moment matrix invertibility) For any $\boldsymbol{x} \in \bar{\Omega}$, a necessary condition for non-singularity of $\boldsymbol{M}(\boldsymbol{x})$ is $|\mathrm{S}(\boldsymbol{x})| \geq N_{p,d}$. A sufficient condition for non-singularity of $\boldsymbol{M}(\boldsymbol{x})$is the existence of a $\pi_{p,d}$-unisolvent subset in $\mathrm{S}(\boldsymbol{x})$.*

It may be noted that the positivity of the kernel functions at points in $\mathrm{S}(\boldsymbol{x})$ plays an important role in the above theorem [Armentano (2001)]. Also, if $d=1$ then the necessary condition is also sufficient. The unisolvency condition is purely a geometric condition on the arrangement of points in $\mathrm{S}(\boldsymbol{x})$ independent of the basis of $\pi_{p,d}$ chosen for the polynomial reproduction in Eq. (C.3). A condition for Z to admit a unique polynomial interpolation is the satisfaction of the *geometric characterization* (GC_p) *condition for a lattice* by Z [Chung and Yao (1977); Jesús and Godés (2006)]. Condition GC_p for Z states: Corresponding to each point z_i, there exists a set of p distinct hyperplanes $\{G_{il}\}_{l=1}^{p}$ such that (i) z_i does not lie on any of these hyperplanes, and (ii) all the other points in Z lie on at least one of these hyperplanes, i.e. $z_j \in \bigcup_{l=1}^{p} G_{il} \Leftrightarrow i \neq j$. It is easy to verify that $L_p(\Delta_d)$ satisfies condition GC_p with the hyperplanes appropriately selected from $\bigcup_{j=0}^{d}\left\{\lambda_j = p'/p : p' \in J_{p-1}^{0}\right\}$. Alternatively, Z admits a unique polynomial interpolation if it forms a system of order p [Gasca and Maeztu (1982); Carnicer, Gasca (2001)]. In practice, application of any of the above tests is not straightforward and thus explicit known configurations that are $\pi_{p,d}$-unisolvent are sought for in $\mathrm{S}(\boldsymbol{x})$ e.g. $L_p(\Delta_d)$.

Now, if $M(\boldsymbol{x})$ is invertible, then Eq. (C.5) can be solved for $\boldsymbol{x}(\boldsymbol{x}) = \boldsymbol{M}^{-1}(\boldsymbol{x})\boldsymbol{H}(0)$ which on substitution in Eq. (C.3) yields $\varphi_i(\boldsymbol{x}) = w_i(\boldsymbol{x}-\boldsymbol{x}_i)\boldsymbol{H}(\boldsymbol{x}-\boldsymbol{x}_i)^T\boldsymbol{M}^{-1}(\boldsymbol{x})\boldsymbol{H}(0)$ Usually, a repeated use of the Leibniz formula *i.e.*

$$D^{\boldsymbol{\kappa}}(fg) = \sum_{\boldsymbol{\beta}\leq\boldsymbol{\kappa}} C_{\boldsymbol{\beta}}\left(D^{\boldsymbol{\beta}}(f)\right)\left(D^{\boldsymbol{\kappa}-\boldsymbol{\beta}}(g)\right)$$

yields the derivatives of the shape function $D^{\boldsymbol{\kappa}}(\varphi_i), |\boldsymbol{\kappa}| \leq k$ (k being the continuity class of the kernel functions). But in this work, an alternative scheme for computing estimate derivatives ($\mathscr{D}^{\boldsymbol{\alpha}}(\cdot), |\boldsymbol{\alpha}| \leq k$) based on the principle that $\boldsymbol{\alpha}$th derivatives of the shape functions reproduce $\boldsymbol{\alpha}$th derivatives of basis elements in $\pi_{p,d}$ is used [Shaw and Roy (2007)]. Thus $\tilde{u}^{\boldsymbol{\alpha}}(\boldsymbol{x}) = \sum_{i=1}^{N} u(\boldsymbol{x}_i)\mathscr{D}^{\boldsymbol{\alpha}}\varphi_i(\boldsymbol{x})$ with the equations analogous to Eq. (C.3-5) being given by Eq. (C.6-8) as follows,

$$D^{\boldsymbol{\alpha}}(\varphi_i) \sim \mathscr{D}^{\boldsymbol{\alpha}}\varphi_i(\boldsymbol{x}) = w_i(\boldsymbol{x}-\boldsymbol{x}_i)\boldsymbol{H}^T(\boldsymbol{x}-\boldsymbol{x}_i)\boldsymbol{c}^{\boldsymbol{\alpha}}(\boldsymbol{x}), \tag{C.6}$$

$$D^{\boldsymbol{\alpha}}\tilde{u}(\boldsymbol{x}) = \sum_{i=1}^{N} w_i(\boldsymbol{x}-\boldsymbol{x}_i)\boldsymbol{H}^T(\boldsymbol{x}-\boldsymbol{x}_i)u(\boldsymbol{x}_i)\boldsymbol{c}^{\boldsymbol{\alpha}}(\boldsymbol{x}) \;\; \forall u \in \pi_{p,d}(\bar{\Omega}) \tag{C.7}$$

$$\boldsymbol{M}(\boldsymbol{x})\boldsymbol{c}^{\boldsymbol{\alpha}}(\boldsymbol{x}) = \left[D^{\boldsymbol{\alpha}}H(\boldsymbol{x})\right]|_{x=0} \tag{C.8}$$

yielding $\mathscr{D}^{\boldsymbol{\alpha}}\varphi_i(\boldsymbol{x}) = w_i(\boldsymbol{x}-\boldsymbol{x}_i)H(\boldsymbol{x}-\boldsymbol{x}_i)^T M^{-1}(\boldsymbol{x})\left[D^{\boldsymbol{\alpha}}H(\boldsymbol{x})\right]|_{x=0}$. The computation of $\mathscr{D}^{\boldsymbol{\alpha}}(\varphi_i)$ does not require the $\boldsymbol{\alpha}$th derivatives of either $M^{-1}(\boldsymbol{x})$ or $w_i(\boldsymbol{x}-\boldsymbol{x}_i)$ unlike the calculation of $D^{\boldsymbol{\alpha}}(\varphi_i)$.

References

Armentano, M. G. (2001): Error estimates in Sobolev spaces for moving least square approximations. *SIAM Journal on Numerical Analysis*, vol. 39, no. 1, pp. 38-51.

Atluri, S. N.; Zhu, T. (1998a): A new meshless local Petrov-Galerkin (MLPG) approach in computational mechanics. *Computational mechanics*, vol. 22, no. 2, pp. 117-127.

Atluri, S. N.; Zhu, T-L. (1998b): A new meshless local Petrov-Galerkin (MLPG) approach to nonlinear problems in computer modeling and simulation. *Computer Modeling and Simulation in Engineering*, vol. 3, pp. 187-196.

Atluri, S. N.; Zhu, T-L. (2000): The meshless local Petrov-Galerkin (MLPG) approach for solving problems in elasto-statics. *Computational Mechanics*, vol. 25, no. 2-3, pp. 169-179.

Babuška, I.; Banerjee, U.; Osborn, J. E. (2003): Meshless and generalized finite element methods: A survey of some major results. *Meshfree methods for partial differential equations*, pp. 1-20. Springer Berlin Heidelberg.

Babuška, I.; Banerjee, U.; Osborn, J. E.; Li, Q. (2008): Quadrature for meshless methods. *International journal for numerical methods in engineering*, vol. 76, no. 9, pp. 1434-1470.

Babuška, I.; Melenk, J. M. (1997): The partition of unity method. *Int. J. Numer. Meth. Engng.*, vol. 40, pp. 727–758.

Belytschko, T.; Black, T. (1999): Elastic crack growth in finite elements with minimal remeshing. *International journal for numerical methods in engineering*, vol. 45, no. 5, pp. 601-620.

Belytschko, T.; Krongauz, Y.; Dolbow, J.; Gerlach, C. (1998): On the completeness of meshfree particle methods. *International Journal for Numerical Methods in Engineering*, vol. 43, no. 5, pp. 785-819.

Belytschko, T.; Krongauz, Y; Organ, D.; Fleming, M.; Krysl, P. (1996). Meshless methods: an overview and recent developments. *Computer methods in applied mechanics and engineering*, vol. 139, no. 1, pp. 3-47.

Belytschko, T.; Lu, Y. Y.; Gu, L. (1994): Element-free Galerkin methods. *International journal for numerical methods in engineering*, vol. 37, no. 2, pp. 229-256.

Belytschko, T.; Organ, D.; Krongauz, Y. (1995): A coupled finite element-element-free Galerkin method. *Computational Mechanics*, vol. 17, no. 3, pp. 186-195.

Carnicer, J.; Gasca, M. (2001): A conjecture on multivariate polynomial interpo-

lation. *Rev. R. Acad., Cien. Serie A. Math*, vol. 95, pp. 145-153.

Chen, J-S.; Pan, C.; Wu, C-T.; Liu, W. K. (1996): Reproducing kernel particle methods for large deformation analysis of non-linear structures. *Computer Methods in Applied Mechanics and Engineering*, vol. 139, no. 1, pp. 195-227.

Chung, K. C.; Yao, T. H. (1977): On lattices admitting unique Lagrange interpolations. *SIAM Journal on Numerical Analysis*, vol. 14, no. 4, pp. 735-743.

Ciarlet, P. G. (1978): *The finite element method for elliptic problems*. Elsevier.

Ciarlet, P. G.; Raviart, P. A. (1972): General Lagrange and Hermite interpolation in R^n with applications to finite element methods. *Archive for Rational Mechanics and Analysis*, vol. 46, no. 3, pp. 177-199.

Dahmen, W. (1980): On multivariate B-splines. *SIAM Journal on Numerical Analysis*, vol. 17, no. 2, pp. 179-191.

Dahmen, W. A.; Micchelli, C. A. (1982): On the linear independence of multivariate B-splines, I. triangulations of simploids. *SIAM Journal on Numerical Analysis*, vol. 19, no. 5, pp. 993-1012.

Dahmen, W. A.; Micchelli, C. A. (1983): On the linear independence of multivariate B-splines. II. Complete configurations. *Mathematics of computation*, vol. 41, no. 163, pp. 143-163.

Dahmen, W.; Micchelli, C. A.; Seidel, H-P. (1992): Blossoming begets B-spline bases built better by B-patches. *Mathematics of computation*, vol. 59, no. 199, pp. 97-115.

Duarte, C. A.; Oden, J. T. (1996): Hp clouds-an hp meshless method. *Numerical methods for partial differential equations*, vol. 12, no. 6, pp. 673-706.

Dolbow, J.; Belytschko, T. (1999): Numerical integration of the Galerkin weak form in meshfree methods. *Computational mechanics*, vol. 23, no. 3, pp. 219-230.

Dunavant, D. A. (1985): High degree efficient symmetrical Gaussian quadrature rules for the triangle. *International journal for numerical methods in engineering*, vol. 21, no. 6, pp. 1129-1148.

Fernández-Méndez, S.; Díez, P.; Huerta, A. (2003): Convergence of finite elements enriched with mesh-less methods. *Numerische Mathematik*, vol. 96, no. 1, pp. 43-59.

Fernández-Méndez, S.; Huerta, A. (2004): Imposing essential boundary conditions in mesh-free methods. *Computer methods in applied mechanics and engineering*, vol. 193, no. 12, pp. 1257-1275.

Fleming, M.; Chu, Y. A.; Moran, B.; Belytschko, T.; Lu, Y. Y.; Gu, L. (1997): Enriched element-free Galerkin methods for crack tip fields. *International Journal*

for Numerical Methods in Engineering, vol. 40, no. 8, pp. 1483-1504.

Franssen, M. G. J. (1995): *Evaluation of DMS-splines*. Master's thesis, Eindhoven University of Technology.

Franssen, M.; Veltkamp, R. C.; Wesselink, W. (2000): Efficient evaluation of triangular B-spline surfaces. *Computer Aided Geometric Design*, vol. 17, no. 9, pp. 863-877.

Fries, T-P.; Matthies, H. G. (2003): Classification and overview of meshfree methods. Scientific Computing, Informatikbericht 3.

Gasca, M.; Maeztu, J. I. (1982): On Lagrange and Hermite interpolation in R^k. *Numerische Mathematik*, vol. 39, no. 1, pp. 1-14.

Gingold, R. A.; Monaghan, J. J. (1977): Smoothed particle hydrodynamics-theory and application to non-spherical stars. *Monthly notices of the royal astronomical society*, vol. 181, pp. 375-389.

Hakopian, H. (1982): Multivariate spline functions, B-spline basis and polynomial interpolations. *SIAM Journal on Numerical Analysis*, vol. 19, no. 3, pp. 510-517.

Hakopian, H.; Jetter, K.; Zimmermann, G. (2014): The Gasca–Maeztu conjecture for $n = 5$. *Numerische Mathematik*, vol. 127, no. 4, pp. 685-713.

Han, W.; Meng, X. (2001): Error analysis of the reproducing kernel particle method. *Computer methods in applied mechanics and engineering*, vol. 190, no. 46, pp. 6157-6181.

Hao, S.; Liu, W. K. (2006): Moving particle finite element method with superconvergence: nodal integration formulation and applications. *Computer methods in applied mechanics and engineering*, vol. 195, no. 44, pp. 6059-6072.

Hjelle, Ø.; Dæhlen, M. (2006). *Triangulations and applications*. Springer.

Huerta, A.; Fernández-Méndez, S. (2000): Enrichment and coupling of the finite element and meshless methods. *Int. J. Numer. Meth. Engng.*, vol. 48, pp. 1615–1636.

Huerta, A.; Fernández-Méndez, S.; Liu, W. K. (2004): A comparison of two formulations to blend finite elements and mesh-free methods. *Computer methods in applied mechanics and engineering*, vol. 193, no. 12, pp. 1105-1117.

Idelsohn, S. R.; Oñate, E.; Pin, F. D. (2004): The particle finite element method: a powerful tool to solve incompressible flows with free surfaces and breaking waves. *International Journal for Numerical Methods in Engineering*, vol. 61, no. 7, pp. 964-989.

Isaksson, P.; Hägglund, R. (2013): Crack-tip fields in gradient enhanced elasticity. *Engineering Fracture Mechanics*, vol. 97, pp. 186-192.

Jesús, C.; Godés, C. (2006): Geometric characterization and generalized principal lattices. *Journal of Approximation Theory*, vol. 143, no. 1, pp. 2-14.

Li, S.; Hao, W.; Liu, W. K. (2000): Mesh-free simulations of shear banding in large deformation. *International Journal of solids and structures*, vol. 37, no. 48, pp. 7185-7206.

Li, S.; Liu, W. K. (2002): Meshfree and particle methods and their applications. *Applied Mechanics Reviews*, vol. 55, no. 1, pp. 1-34.

Liu, W. K.; Han, W.; Lu, H.; Li, S.; Cao, J. (2004): Reproducing kernel element method. Part I: Theoretical formulation. *Computer Methods in Applied Mechanics and Engineering*, vol. 193, no. 12, pp. 933-951.

Liu, W. K.; Jun, S.; Zhang, Y. F. (1995): Reproducing kernel particle methods. *International journal for numerical methods in fluids*, vol. 20, no. 8-9, pp. 1081-1106.

Liu, W. K.; Li, S.; Belytschko, T. (1997): Moving least-square reproducing kernel methods (I) methodology and convergence. *Computer Methods in Applied Mechanics and Engineering*, vol. 143, no. 1, pp. 113-154.

Lucy, L. B. (1977): A numerical approach to the testing of the fission hypothesis. *The astronomical journal*, vol. 82, pp. 1013-1024.

Melenk, J. M. (2005): On approximation in meshless methods. *Frontiers of numerical analysis*, pp. 65-141. Springer Berlin Heidelberg.

Melenk, J. M.; Babuška, I. (1996): The partition of unity finite element method: basic theory and applications. *Computer methods in applied mechanics and engineering*, vol. 139, no. 1, pp. 289-314.

Meyling, R. H. J. G. (1987): An algorithm for constructing configurations of knots for bivariate B-splines. *SIAM journal on numerical analysis*, vol. 24, no. 3, pp. 706-724.

Micchelli, C. A. (1980): A constructive approach to Kergin interpolation in R^k: Multivariate B-splines and Lagrange Interpolation. *Rocky Mountain Journal of Mathematics*, vol. 10, no. 3, pp. 485-497.

Moszynska, M. (2006): *Selected topics in convex geometry*. Birkhäuser.

Nayroles, B.; Touzot, G.; Villon, P. (1992): Generalizing the finite element method: diffuse approximation and diffuse elements. *Computational mechanics*, vol. 10, no. 5, pp. 307-318.

Nguyen, V. P.; Rabczuk, T.; Bordas, B.; Duflot, M. (2008): Meshless methods: a review and computer implementation aspects. *Mathematics and computers in simulation*, vol. 79, no. 3, pp. 763-813.

Niceno, B. (2001): Easymesh: a free two-dimensional quality mesh generator based on Delaunay triangulation. Available in *http://www.dinma. univ. trieste. it/nirftc/research/easymesh/Default.htm*

Onate, E.; Idelsohn, S.; Zienkiewicz, O. C.; Taylor, R. L. (1996): A finite point method in computational mechanics. Applications to convective transport and fluid flow. *International Journal for Numerical Methods in Engineering*, vol. 39, no. 22, pp. 3839-3866.

Rabczuk, T.; Xiao, S. P.; Sauer, M. (2006): Coupling of meshfree methods with finite elements: basic concepts and test results. *Communications in Numerical Methods in Engineering*, vol. 22, no. 10, pp. 1031-1065.

Rajan, V. T. (1994): Optimality of the Delaunay triangulation in R^d. *Discrete & Computational Geometry*, vol. 12, no. 1, pp. 189-202.

Rippa, S. (1990): Minimal roughness property of the Delaunay triangulation. *Computer Aided Geometric Design*, vol. 7, no. 6, pp. 489-497.

Seidel, H-P. (1992): Polar forms and triangular B-spline surfaces. Blossoming: The New Polar-Form Approach to Spline Curves and Surfaces. SIGGRAPH'91 Course Notes #26. pp. 235-286. World Scientific Publishing Co.

Shaw, A.; Banerjee, B.; Roy, D. (2008): A NURBS-based parametric method bridging mesh-free and finite element formulations. *Computer Modeling in Engineering and Sciences (CMES)*, vol. 26, no. 1.

Shaw, A.; Roy, D. (2007): A NURBS-based error reproducing kernel method with applications in solid mechanics. *Computational Mechanics*, vol. 40, no. 1, pp. 127-148.

Shaw, A.; Roy, D. (2008): NURBS-based parametric mesh-free methods. *Computer methods in applied mechanics and engineering*, vol. 197, no. 17, pp. 1541-1567.

Strouboulis, T.; Copps, K.; Babuška, I. (2000): The generalized finite element method: an example of its implementation and illustration of its performance. *International Journal for Numerical Methods in Engineering*, vol. 47, no. 8, pp. 1401-1417.

Sunilkumar, N.; Lalmoni, G., Roy, D.; Reid, S. R.; Vasu, R. M. (2012): Wrinkled and slack membranes: nonlinear 3D elasticity solutions via smooth DMS-FEM and experiment. *International Journal for Numerical Methods in Engineering*, vol. 90, no. 10, pp. 1233-1260.

Sunilkumar, N.; Roy. D. (2010): A smooth finite element method based on reproducing kernel DMS-splines. *Computer Modeling in Engineering and Sciences (CMES)*, vol. 65, no. 2, pp. 107-153.

Sunilkumar, N.; Roy, D.; Reid, S. R. (2012): Smooth DMS–FEM: A new approach to solving nearly incompressible nonlinear elasto-static problems. *International Journal of Mechanical Sciences* vol. 54, no. 1, pp. 136-155.

Tang, Z.; Shen, S.; Atluri, S. N. (2003): Analysis of materials with strain-gradient effects: A meshless local Petrov-Galerkin (MLPG) approach, with nodal displacements only. *Computer Modeling in Engineering and Sciences*, vol. 4, no. 1, pp. 177-196.

Ventura, G.; Xu, J. X.; Belytschko, T. (2002): A vector level set method and new discontinuity approximations for crack growth by EFG. *International Journal for numerical methods in engineering*, vol. 54, no. 6, pp. 923-944.

Yagawa, G.; Yamada, T. (1996): Free mesh method: a new meshless finite element method. *Computational Mechanics*, vol. 18, no. 5, pp. 383-386.

Zuppa, C. (2003a): Good quality point sets and error estimates for moving least square approximations. *Applied Numerical Mathematics*, vol. 47, no. 3, pp. 575-585.

Zuppa, C. (2003b): Error estimates for moving least square approximations. *Bulletin of the Brazilian Mathematical Society*, vol. 34, no. 2, pp. 231-249.